

DISK LOSS AND DISK RENEWAL PHASES IN CLASSICAL BE STARS I: ANALYSIS OF LONG-TERM SPECTROPOLARIMETRIC DATA

JOHN P. WISNIEWSKI^{1,2}, ZACHARY H. DRAPER¹, KAREN S. BJORKMAN³, MARILYN R. MEADE⁴,
JON E. BJORKMAN³, ADAM F. KOWALSKI¹*Accepted in ApJ Dec 8, 2009*

ABSTRACT

Classical Be stars are known to occasionally transition from having a gaseous circumstellar disk (“Be phase”) to a state in which all observational evidence for the presence of these disks disappears (“normal B-star phase”). We present one of the most comprehensive spectropolarimetric views to date of such a transition for two Be stars, π Aquarii and 60 Cygni. 60 Cyg’s disk loss episode was characterized by a generally monotonic decrease in emission strength over a time-scale of ~ 1000 days from the maximum V-band polarization to the minimum H α equivalent width, consistent with the viscous time-scale of the disk, assuming $\alpha \sim 0.14$. π Aqr’s disk loss was episodic in nature and occurred over a time-scale of ~ 2440 days. An observed time lag between the behavior of the polarization and H α in both stars indicates the disk clearing proceeded in an “inside-out” manner. We determine the position angle of the intrinsic polarization to be $166.7 \pm 0.1^\circ$ for π Aqr and $107.7 \pm 0.4^\circ$ for 60 Cyg, and model the wavelength dependence of the observed polarization during the quiescent diskless phase of each star to determine the interstellar polarization along the line of sight. Minor outbursts observed during the quiescent phase of each star shared similar lifetimes as those previously reported for μ Cen, suggesting that the outbursts represent the injection and subsequent viscous dissipation of individual blobs of material into the inner circumstellar environments of these stars. We also observe deviations from the mean intrinsic polarization position angle during polarization outbursts in each star, indicating deviations from axisymmetry. We propose that these deviations might be indicative of the injection (and subsequent circularization) of new blobs into the inner disk, either in the plane of the bulk of the disk material or in a slightly inclined (non-coplanar) orbit.

Subject headings: circumstellar matter — stars: individual (pi Aquarii) — stars: individual (60 Cygni)

1. INTRODUCTION

Since the pioneering work of Struve (1931), a sub-set of B-type main sequence stars rapidly rotating at velocities ranging from $>40\%$ (for early-type B stars; Cranmer 2005) to possibly 100% of the critical rate (Townsend et al. 2004) have been identified. Photometric, spectroscopic, polarimetric, and interferometric observations of these so called classical Be stars indicate that they are characterized by the presence of a geometrically flattened, circumstellar decretion disk (for a recent review see Porter & Rivinius 2003). While for single stars the origin of the gas in these disks is agreed to be material ejected from the stellar photosphere, the precise mechanism for forming these disks remains elusive. Suggested disk formation mechanisms include the compression of stellar winds (“WCD” model; Bjorkman & Cassinelli 1993), potentially aided by the channeling of magnetic fields (Cassinelli et al. 2002; Brown et al. 2008), as well as the viscous decretion disk model (Lee et al. 1991), which could be fed via non-radial pulsational events (Cranmer 2009) similar to those which have been observed in several Be stars (Rivinius et al. 1998; Neiner et al. 2002).

Classical Be stars are known to exhibit variability on a multitude of time-scales and amplitudes, includ-

ing short-term (hours to weeks) polarimetric variability (Carciofi et al. 2007), multi-periodic short-term spectroscopic variability arising from non-radial pulsations (Rivinius et al. 1998), and long-term (several to tens of years) cyclical spectroscopic variability originating from one-armed density waves in the disk (Okazaki 1991; Stefl et al. 2009). Arguably the most dramatic type of variability observed is the aperiodic “Be to normal B to Be” transition whereby classical Be stars dissipate (i.e. lose) their disks, and will often begin to regenerate a new disk after a period of relative quiescence (see e.g. Underhill & Doazan 1982 and references therein). While several individual stars have been observed to experience this transition one or more times (Underhill & Doazan 1982; Doazan et al. 1983; Clark et al. 2003; Vinicius et al. 2006), it is not known whether there is a characteristic time-scale for disk-loss and regeneration that would suggest a singular disk formation mechanism or whether each event is unique. Although their sample size is small, recent monitoring of eight open clusters by McSwain et al. (2009) has revealed a surprising 12 new transient Be stars out of a sample of 296 stars monitored, suggesting that disk-loss/renewal episodes may be a prevalent phenomenon. Be stars experiencing a “Be to normal B to Be” transition are clearly of significant astrophysical importance as they pro-

¹ Department of Astronomy, University of Washington, Box 351580 Seattle, WA 98195, USA, jwisniei@u.washington.edu, zhd@uw.edu, adamfk@u.washington.edu

² NSF Astronomy & Astrophysics Postdoctoral Fellow

³ Ritter Observatory, Department of Physics & Astronomy, Mail Stop 113, University of Toledo, Toledo, OH 43606, karen.bjorkman@utoledo.edu, jon@physics.utoledo.edu

⁴ Space Astronomy Lab, University of Wisconsin-Madison, 1150 University Avenue, Madison, WI 53706, meade@astro.wisc.edu

vide observational evidence of how Be disks form, thereby constraining theoretical efforts to identify the disk formation mechanism.

Polarimetry has an established history of providing a unique diagnostic in identifying and studying the detailed circumstellar environments of both individual classical Be stars (Quirrenbach et al. 1997; Wood et al. 1997; Clarke & Bjorkman 1998) and larger statistical ensembles (Coyne & Kruszewski 1969; McLean & Brown 1978; Poeckert et al. 1979; Wisniewski et al. 2007b). Electron scattering modified by pre- or post-scattering absorption by hydrogen atoms in the disk produces the characteristic wavelength dependent polarization signature of Be stars (Wood et al. 1996a,b). Modeling such data yields information about the density in the inner region of these disks (Wood et al. 1997; Carciofi et al. 2009) and has been used, along with interferometric observations, to confirm that the disks are geometrically thin (Quirrenbach et al. 1997).

The two stars we examine in this paper, 60 Cygni and π Aquarii, are well known classical Be stars. 60 Cyg (HD 200310) is a B1Ve classical Be star (Slettebak 1982). Periodic radial velocity variations of H α and He I 6678 Å suggest that the star might be a spectroscopic binary having a period of 146.6 ± 0.6 days, while 1.064 day line profile variations and 0.2997 day photometric variations may be caused by non-radial pulsations (Koubsky et al. 2000). Koubsky et al. (2000) present evidence that the star has experienced disk-loss and subsequent regeneration in the past (see e.g. their Figure 1), with photometric variability positively correlated with H α emission strength; however, they neither discuss the detailed time-scale for these events nor publish their data in sufficient format to derive this information. π Aqr (HD 212571) is a B1 III-IVe classical Be star (Slettebak 1982). As discussed in Bjorkman et al. (2002) and references therein, π Aqr’s most recent disk likely developed in the early 1950s and persisted until 1996. Analysis of spectroscopic data obtained after 1996, when the star was in a diskless “normal B star” phase, revealed the star has a close binary companion with an orbital period of 84.1 days (Bjorkman et al. 2002), which might be engaged in variable mass transfer with the primary.

In this paper, we present and analyze an extensive spectropolarimetric dataset which covers the disk-loss phase transition in two Be stars. In Section 2, we outline our new spectroscopic and spectropolarimetric observations of 60 Cyg and π Aqr. We analyze the time evolution of our spectroscopic data in Section 3.1 and the time evolution of our polarimetric data in Section 3.2. A thorough discussion of the interstellar polarization along the line of sight to 60 Cyg and π Aqr is presented in Section 3.3. Finally we offer a detailed discussion and interpretation of our results in Section 4 and suggest future work in Section 5.

2. OBSERVATIONS AND DATA REDUCTION

The spectropolarimetric data analyzed in this study were obtained by the University of Wisconsin’s (UW) HPOL spectropolarimeter, mounted on UW’s 0.9m Pine Bluff Observatory (PBO) telescope. π Aquarii was observed on 127 nights between 1989 August 8 and 2004 October 10 while 60 Cygni was observed on 35 nights between

1992 August 3 and 2004 September 26 (see Tables 1 and 2). Data obtained before 1995 were recorded using a dual Reticon array detector spanning the wavelength range of 3200 - 7600Å with a spectral resolution of 25Å (Wolff et al. 1996). Since 1995, HPOL has been equipped with a 400 x 1200 pixel CCD and two gratings which provide coverage from 3200 -6020Å and 5980 - 10,500Å at a resolution of 7Å below 6000Å and 10Å above this point (Nordsieck & Harris 1996). Further details about HPOL can be found in Nook (1990), Wolff et al. (1996), and Harries et al. (2000), and all HPOL data obtained between 1989-1994 are publically available from the Multimission Archive at STScI (MAST) website: <http://archive.stsci.edu/hpol>.

HPOL data were reduced, processed, and analyzed using REDUCE, a spectropolarimetric software package developed by the University of Wisconsin-Madison (see Wolff et al. 1996). Routine monitoring of unpolarized standard stars at PBO has enabled the instrumental polarization to be carefully calibrated; the residual instrumental systematic errors depend mildly on the date of the observations, but range from 0.027-0.095% in the U-band, 0.005-0.020% in the V-band, and 0.007-0.022% in the I-band. HPOL spectroscopic data are not calibrated to an absolute flux level due to the nonphotometric skies typically present during the observations (Harries et al. 2000).

We supplement our HPOL spectroscopic observations of 60 Cyg with 65 nights of spectra obtained from 1998 August 26 to 2006 December 9 using the fiber-fed echelle spectrograph of the 1.0m Ritter Observatory at the University of Toledo (Table 1). These spectra span nine non-adjacent 70 Å wide orders in the range 5285-6595Å with $R \sim 26,000$. The data were reduced in IRAF using standard spectroscopic techniques, including bias correction, flat-fielding, and wavelength calibration. Additional details about Ritter data are given in Morrison et al. (1997).

Our HPOL polarimetric observations of π Aqr are also supplemented by literature V-band polarization measurements (Table 2; McDavid 1986, 1990, 1994, 1999). Moreover, both our 60 Cyg and π Aqr data are supplemented by unpublished observations made with the Lyot Polarimeter at PBO between 1979-1987 (Table 3), which spanned an effective wavelength range of 4800-7600 Å in 1979, 4800-8200 Å in 1980, and 4600-7200 Å in 1987. Further details about the PBO Lyot Polarimeter can be found in Lupie & Nordsieck (1987); Whitney & Clayton (1989); and Nook et al. (1990).

3. DATA ANALYSIS

3.1. H- α Spectroscopy

We begin our analysis by determining the H α equivalent width (EW) of all of our spectroscopic data, with no correction for the constant underlying photospheric absorption line present. Following continuum normalization, the EWs of our Ritter data were computed using *splot* in IRAF⁵. Equivalent width errors were computed using $\sigma^2 = N[h_\lambda/(S/N)]^2(f_*/f_c)$, where N is the number of pixels across the H α line, h_λ is the dispersion in Å⁻¹, f_* is the flux in the line, f_c is the flux in the continuum, and S/N is the signal-to-noise ratio calculated in a line-free region of the spectra neighboring the H α line (Chalabaev & Maillard

⁵ IRAF is distributed by the National Optical Astronomy Observatory, which is operated by the Association of Universities for Research in Astronomy, Inc., under contract with the National Science Foundation.

1983). For our HPOL data, the spectral regions 6350-6450 and 6700-6800Å were used to constrain the continuum flux around H α while the region 6520-6620Å was used to measure the H α line flux. Three nights of our π Aqr HPOL dataset (MJD 2452860, 2452906, 2453181) suffered from extremely poor wavelength calibration, requiring us to shift the three spectra from these nights by ~ 80 Å.

Our EW data are compiled in Table 1 (60 Cyg) and Table 2 (π Aqr). The EWs of our HPOL and Ritter observations of 60 Cyg are systematically offset from one another. This is likely caused both by the different resolution of the instruments used and by the continuum in our low-resolution HPOL spectra not being perfectly fit via the linear function derived from our 2 continuum filters. We stress however that this constant offset has no effect on our analysis or conclusions. Comparison of four nights in which both instruments obtained spectroscopic observations indicates this offset is ~ 1.9 Å; for plotting purposes only (Figure 1), we have added a constant offset of 1.9Å to our HPOL EWs measurement. Note that no offset has been added to the tabulated measurements in Table 1.

3.1.1. 60 Cyg

Figure 1 clearly demonstrates that 60 Cyg experienced a fundamental change at H α throughout our 14 years of spectroscopic monitoring data, during which the line changed from absorption to emission to absorption. Koubsky et al. (2000) qualitatively report a potentially similar event prior to our observations, but they did not publish their detailed EW measurements and only referred to the disk as being in “strong emission, an intermediate state, and pure absorption”, thereby precluding a more comprehensive comparison of the events. Our data indicate that it took ~ 870 days for 60 Cyg’s disk to transform from its strongest H α emission state (1998 December 24; Table 1) to its lowest state of pure absorption, the latter of which we interpret as the time when the disk had completely dissipated (2001 May 9; Table 1). Inspection of the decline state, seen in the right-panel of Figure 1, reveals that to first order the disk’s emission strength followed a monotonic decrease void of any dramatic outbursts. After reaching its low state in 2001 May, 60 Cyg remained at a moderately low state characterized by occasional minor increases in the H α EW through the last of our observations in 2006 December.

Binary companions can influence the circumstellar disks of Be stars in several ways. They are believed to influence the behavior of global disk oscillations (Oktariani & Okazaki 2009), truncate the outer disk (Carciofi et al. 2009), and potentially trigger mass-loss events from the central star for systems in very eccentric orbits (e.g. δ Sco; Miroshnichenko et al. 2001). Assuming the range of primary and secondary masses for 60 Cyg given by Koubsky et al. (2000) and a circular orbit, 60 Cyg’s disk could be truncated at the tidal distance of ~ 120 -135 R_{sun} , assuming the tidal radius is $\sim 0.9 R_{Roche}$ (valid for small mass ratios; Whitehurst & King 1991) and using the Roche radius approximation of Eggleton (1983). Aside from this possible truncation, we suggest it is unlikely that the binary companion is a fundamental contributor to 60 Cyg’s disk-loss event. The time-scale of the disk-loss event (~ 870 days) corresponds to almost 6 com-

plete orbits of the binary companion (assuming a 146.6 day period; Koubsky et al. 2000), suggesting that the binary does not influence the primary star (or its disk) in a manner similar to the highly eccentric δ Sco system (Miroshnichenko et al. 2001).

3.1.2. π Aqr

The time evolution of the H α EW of π Aqr (Figure 2) also provides clear evidence of a disk-loss event, at a higher sampling frequency than available in previous publications (Bjorkman et al. 2002). Our data indicate that it took at least ~ 2440 days for π Aqr’s disk to transform from its strongest state observed during our time coverage (1989 October 26; EW = -24.6 Å Table 2) to the likely start of its minimum state of pure absorption (1996 July 4; EW = 4.1 Å Table 2). While the overall behavior of π Aqr’s decline phase shows a mostly monotonic decline in emission strength (left panel, Figure 2), similar to that seen for 60 Cyg, there is clear evidence of two significant interruptions to this trend. The decline of π Aqr’s H α emission experienced a ~ 220 day flattening event beginning on 1991 May 12 (JD 2448389) and a ~ 200 day event beginning on 1994 June 5 (JD 2449509), during which its EW not only flattened but exhibited evidence of temporarily increasing in emission strength (right panel, Figure 2).

The time-scale for π Aqr’s disk-loss episode (~ 2440 days) corresponds to roughly 29 complete orbits of its known binary companion (assuming a 84.1 day period; Bjorkman et al. 2002), which suggests that the passage of the binary was not responsible for triggering the disk-loss episode. Assuming the range of primary and secondary masses for π Aqr given by Bjorkman et al. (2002) and a circular orbit, we calculate that π Aqr’s disk could be truncated at the tidal distance of 80-89 R_{sun} , assuming the tidal radius is $\sim 0.9 R_{Roche}$ (Whitehurst & King 1991) and using the Roche radius approximation of Eggleton (1983). Aside from this possible truncation, we suggest it is unlikely that the binary companion influences the primary star (or its disk) in a manner similar to the highly eccentric δ Sco system (Miroshnichenko et al. 2001).

After the likely start of its minimum “pure absorption” state in 1996 July, π Aqr’s H α EW remained generally unchanged until 2001 November, at which time a minor filling-in of the photospheric absorption line occurred and lasted until 2002 June. A similar strengthening event appeared to begin at or around 2003 October and persisted through our final observation on 2004 October, though the H α emission strength never approached the values observed during the star’s previous strong-disk phase.

3.2. Total V-band Polarization

Theoretical models predict that the predominant physical locations in the disk at which H α photons are emitted and at which photons are scattered to produce the observed polarization differs in Be stars, with the polarization produced in the very inner disk region and H α photons coming from throughout a much more extended radial distance (Carciofi & Bjorkman 2006; Carciofi et al. 2009). For example, application of these models to observational data for the Be star ζ Tau (Wisniewski et al. 2007a; Steff et al. 2009) suggest that while the scattering events producing polarized photons are produced within

a few stellar radii, $H\alpha$ photons are emitted over a substantially broader region of the disk, extending out to ~ 40 stellar radii. Therefore, our spectropolarimetric dataset provides unique simultaneous insight into the long-term behavior of the inner versus outer regions of 60 Cyg’s and π Aqr’s circumstellar disks. To facilitate comparison with our $H\alpha$ EW data, we have binned our spectropolarimetric data to replicate the Johnson V-band filter.

3.2.1. 60 Cyg

The time evolution of 60 Cyg’s observed (intrinsic and ISP) V-band polarization is depicted in the top panels of Figure 1 and tabulated in Table 1. While the observed magnitude of polarization mimics the similar long-term trend as the strength of the $H\alpha$ line emission, the maximum $H\alpha$ emission lags the peak polarization observed on 1998 August 24 by ~ 120 days, as depicted by the first two vertical lines in the right panels of Figure 1. Similarly, the onset of the minimum $H\alpha$ EW (third vertical line, Figure 1) lagged the onset of the polarization low-state by ~ 190 days. Such a time lag between the onset of polarimetric and spectroscopic features in Be stars has been previously reported in the literature (see e.g. Poeckert & Marlborough 1978a,b) and is indicative that the clearing of the disk proceeds in an “inside-out” manner. If we assume that the time period immediately following the polarization maximum denotes the beginning of the disk-loss transformation, then the full time-scale for disk loss is simply the summation of the $H\alpha$ EW decline time-scale plus the polarization time lag (~ 870 days + ~ 120 days), ~ 1000 days. This disk loss time-scale is similar to the ~ 700 day time-scale Poeckert et al. (1982) noted for the loss of omicron And, using the same definition of the start and termination of the disk-loss phase.

In Section 3.1.1 we noted the presence of minor, temporary increases in the $H\alpha$ EW after 60 Cyg reached its diskless low state. Inspection of Figure 1 illustrates that one of these EW events near 2004 Aug 30-31 was accompanied by a $\sim 0.3\%$ V-band polarimetric outburst, strengthening our interpretation that these minor outbursts represent tenuous attempts of the system to reform a gaseous circumstellar disk.

Though not plotted in Figure 1 for aesthetic reasons, the PBO Lyot polarization observation from 1987 (Table 3), which encompasses the V-band, is consistent with HPOL polarimetry obtained during epochs in which 60 Cyg was characterized by a strong disk. These data are also consistent with the results of Koubsky et al. (2000), who reported strong $H\alpha$ emission present before (early 1980s) and after (later 1980s) our PBO Lyot observation.

3.2.2. π Aqr

The time evolution of π Aqr’s observed V-band polarization, depicted in the top panels of Figure 2 and tabulated in Table 2, exhibits a substantially more complex morphology during the star’s disk-loss episode as compared to 60 Cyg. Archival V-band polarization prior to the onset of our observations (McDavid 1986, 1990), plotted as open circles in Figure 2, indicate that the disk was in a stable high state between 1985-1987. Figure 2 clearly shows that the ~ 2440 day long decline of the $H\alpha$ EW was interrupted by two massive polarimetric outbursts. The ~ 390 day long

first polarimetric event, demarked by the first and second vertical lines in the right panels of Figure 2, is clearly related to the ~ 220 day long first $H\alpha$ EW event noted in Section 3.1.2. The ~ 730 day long second polarimetric event, demarked by the third and fourth vertical lines in the right panels of Figure 2, is similarly related to the ~ 200 day second interruption of the $H\alpha$ EW decline noted in Section 3.1.2, during which the EW briefly began to re-strengthen.

Given the complex morphology of both the V-band polarization outbursts and the interruptions of the $H\alpha$ EW decline, it is more difficult to quantify the exact time lag between the onset of polarimetric features and the corresponding effects in $H\alpha$. However, inspection of Figure 2 clearly shows that such a time lag does exist; for example, the total V-band polarization reaches its low state much earlier than the time at which the $H\alpha$ EW reaches its low state. Similar to our interpretation of our 60 Cygni data, we deduce this time lag as evidence that π Aqr’s disk cleared in an “inside-out” fashion.

In Section 3.1.2 we noted the presence of two minor, temporary increases in the $H\alpha$ EW after the polarimetric data indicated that π Aqr had reached its quiescent, diskless state. We note that the final EW increase, which began in 2003 October and was still ongoing at the termination of our observational data in 2004 October, coincided with a corresponding temporary increase in the system’s total V-band polarization, which peaked at 0.2% above the background interstellar polarization level on 2004 August 29. We observed no increase in the polarization corresponding to the 2001 November - 2002 June $H\alpha$ EW outburst, and speculate that we missed observing the onset of this event due to the sparse time sampling of our polarimetric observations during this epoch.

Though not plotted in Figure 1 for aesthetic reasons, the PBO Lyot polarization observations from 1979-1980 (Table 3), which encompass the V-band, are consistent with HPOL polarimetry obtained during epochs in which π Aqr was characterized by a strong disk and also consistent with the general level of V-band polarization in the late 1970s presented by Bjorkman et al. (2002).

3.3. Interstellar Polarization

While polarimetry can be used as a unique diagnostic tool to investigate the properties of astrophysical objects, proper interpretation of these data is inherently difficult, as observations can contain contributions which are both intrinsic and interstellar in origin. The identification and complete removal of the interstellar polarization component (hereafter ISP), and a thorough understanding of the accuracy of this removal, is thus a critical first step in interpreting polarimetric data. As detailed by McLean & Brown (1978) and discussed in Quirrenbach et al. (1997), there are three techniques commonly used to determine ISP along a line of sight: field star studies, emission line polarization analysis, and wavelength dependence studies.

3.3.1. Field Star Technique

Field star studies are the most basic of the ISP separation techniques, and due to their large uncertainties, they are most useful when used in combination with other

methods. The technique involves averaging the observed polarization of stars at the similar distances to and small angular separations from the science target. It inherently assumes the existence of uniform interstellar medium conditions in the vicinity of the target and also assumes that the field stars themselves are devoid of any intrinsic polarization component. While the technique can be highly successful when used to analyze the ISP properties of open clusters, where one can assume all members are located at the same distance and there are sufficient numbers of stars to lessen the effects of small intrinsic polarization components in the field stars by brute force averaging of a large number of stars (see e.g. Wisniewski et al. 2007b), the application of the technique to isolated stars often yields imprecise ISP estimates (see McLean & Clarke 1979, Bjorkman et al. 1998, and Wisniewski et al. 2006).

We were able to identify seven non-emission line stars with polarimetric data in the catalog of Mathewson & Ford (1970) spatially near the position of π Aqr on the sky which appeared to be suitable field stars (see Table 4). Averaging these field stars yields the ISP parameters of $P_{ism} = 0.47\%$ at $\theta_{ism} = 130.1^\circ$. As we will show in Section 3.3.3, this initial ISP estimate does not fully remove the interstellar polarization component from our data; hence, we do not adopt these values as our final ISP determination along the line of sight to π Aqr.

Using the polarization catalog of Heiles (2000), we were only able to identify one non-emission line star with suitable polarimetric data having a similar distance as 60 Cyg (418 pc, Perryman et al. 1997; see Table 4). As seen in Figure 3, most of the stars spatially coincident with 60 Cyg are in the foreground; moreover, the one star at a similar distance (250 - 550 pc) as 60 Cyg exhibits a significantly different polarization. We conclude that the field star technique fails to yield a useful estimate of the ISP along the line of sight to 60 Cyg.

3.3.2. $H\alpha$ Line Depolarization

If one assumes that the physical location of the emitting region of emission lines in an astrophysical object lies exterior to the region producing any intrinsic polarization, as suggested by Harrington & Collins (1968), one can measure the polarization across emission lines such as $H\alpha$ and use these values as measures of the ISP along the line of sight. While this technique has been successfully employed for a wide variety of objects (Nordsieck et al. 2001; Meyer et al. 2002; Wisniewski et al. 2006), McLean & Clarke (1979) note that the semi-empirical relationship used to isolate ISP via this technique is questionable and subject to numerous complications. Quirrenbach et al. (1997) remark that the technique's assumption of a constant intrinsic position angle across $H\alpha$ is also doubtful and note that their own spectropolarimetric observations show $H\alpha$ is not completely unpolarized. Poeckert et al. (1979), Oudmaijer et al. (2005), and Harrington & Kuhn (2009) also demonstrate that Be stars can exhibit intrinsic line polarization features. The reliability of this technique is therefore uncertain at best.

To apply this technique to our data, we first created artificial filters which sampled regions within the $H\alpha$ line core (6520 - 6620Å) and continuum on both sides of the line

(6350 - 6450 Å and 6700 - 6800 Å). We then determined the polarization within the $H\alpha$ line and its nearby continuum, using these filters, for all data which showed clear spectroscopic evidence of having $H\alpha$ in emission. We plotted the continuum and line polarizations for each observation of π Aqr and 60 Cyg on separate Stokes Q-U diagrams, and looked for the standard evidence of full line depolarization effects. Careful inspection of these figures revealed that the lines connecting each continuum-line observation set pointed in a different direction and that the $H\alpha$ line polarization measurements were not clustered around one central location. These trends indicated that intrinsic polarization within the line was likely contaminating our data, thereby precluding our use of $H\alpha$ line depolarization as an ISP constraint for both π Aqr and 60 Cyg.

3.3.3. Serkowski Law Fitting

The wavelength dependence of interstellar polarization can be expressed by the empirical Serkowski law (Serkowski et al. 1975), as modified by Wilking et al. (1982): $P(\lambda) = P_{max} \exp[-K \ln^2(\lambda_{max}/\lambda)]$. In the absence of additional constraints, one can attempt to determine the ISP along the line of sight to an object containing both interstellar and intrinsic polarization if one has *a priori* knowledge of the position angle of the intrinsic polarization component (see e.g. Poeckert et al. 1979). Our π Aqr and 60 Cyg spectropolarimetric data are particularly unique in that they span an era in which each star enters a "normal B star" phase in which all observational evidence of the presence of a disk, including an intrinsic polarization component, had disappeared. The remnant polarization in these low-state data can be assumed to be fully interstellar in origin, thereby providing us the opportunity to accurately fit their wavelength dependence using a modified Serkowski law.

We begin by plotting our entire V-band datasets for 60 Cyg and π Aqr on a Stokes Q-U diagram as seen in Figures 4 and 5 respectively, where

$$Q = P \cos(2\theta) \quad (1)$$

$$U = P \sin(2\theta) \quad (2)$$

$$P = (Q^2 + U^2)^{0.5} \quad (3)$$

$$\theta = 0.5 \tan^{-1}(U/Q) \quad (4)$$

The time evolution of the polarimetric data in each of these figures follows a strict linear trend, indicating a constant scattering angle (i.e. position angle) regardless of the magnitude of polarization, as is expected for electron scattering in a gaseous circumstellar disk. The slope of the best fit linear regression to our 60 Cyg data (Figure 4) was 0.71 ± 0.02 . This indicates that the intrinsic polarization position angle for 60 Cyg is $\theta_* = 107.7 \pm 0.4^\circ$, and under the typical assumption that the maximum polarization occurs for 90° scattering it also implies that 60 Cyg's disk is oriented at a position angle of $\theta_{disk} = 17.7^\circ$ on the sky (measured in the convention of North to East). The slope of the best fit linear regression to our π Aqr data (Figure 5) was -0.50 ± 0.01 . This translates into an intrinsic polarization position angle, θ_* of $166.7 \pm 0.1^\circ$ for π Aqr, and implies that π Aqr's disk is oriented at a position angle of $\theta_{disk} = 76.7^\circ$ on the sky.

Using an iterative process, we next carefully examined the polarimetric data which corresponded to time-periods in which H α was nearly or completely in absorption to help identify all observations which were devoid of an intrinsic polarization component. Data comprised solely of an interstellar polarization component, which we labeled as “L” for *polarization* low-state in Tables 1 and 2, clearly correlated with one another in a clump on the Stokes Q-U diagram (see e.g. Q \sim 0% and U \sim 0.1% in Figure 4). Recall from Section 3.2 that H- α emission probes a much more extended region of a Be star’s circumstellar environment than optical polarization measurements; therefore, our definition of a *polarization* low-state only establishes that the density of material in the inner disk region dramatically dropped (or was completely cleared) and therefore does not demand that the outer circumstellar environment be similarly completely cleared of disk material. Since the intrinsic polarization arising from classical Be stars follows a tight linear trend, we can effectively isolate the presence of any residual intrinsic polarization in our polarization low-state data by rotating all of our observations by the negative value of the intrinsic polarization position angle.

For 60 Cyg, we rotated our data by -107.7° , thereby placing any small amount of residual intrinsic polarization in the Stokes Q’ parameter (where the prime denotes the rotated frame) and fully isolating the perpendicular component of the interstellar polarization in the Stokes U’ parameter. After co-adding all low state polarization data in this rotated frame, we then fit a modified Serkowski law to the U’ data using the IDL subroutine *mpcurvefit*, as demonstrated in Figure 6, which plots the U’ component of the 60 Cyg data binned to a constant (Poisson photon statistic) polarization error of 0.01%. 60 Cyg’s perpendicular ISP component (U’ data) is clearly well fit by a modified Serkowski law having parameters listed in Table 5. There is very little signal in 60 Cyg’s Q’ component (Figure 4); hence, we could not fit the data with a modified Serkowski law to extract the parallel ISP component. Instead, we overplotted our perpendicular ISP component on our low-state polarization data in the Stokes Q’-U’ parameter space and estimated the lower-limit of the parallel ISP component needed to ensure that our lowest state datapoint was purely interstellar in nature (see dashed line in Figure 7). Our lower limit estimate of the parallel ISP is tabulated in Table 5, along with the total ISP estimate derived from vectorally adding the perpendicular and parallel ISP components. We find the total ISP for 60 Cyg to be characterized by $P_{max} = 0.112\% \pm 0.001\%$, $\lambda_{max} = 6977 \pm 241\text{\AA}$, PA = 41.5° , and K = 1.17. The wavelength dependence of our polarization low state 60 Cyg data after subtraction of this total ISP, seen in Figure 8 binned to a constant polarization error of 0.015%, is centered about Q = 0% and U = 0% and exhibits no significant structure, thereby confirming the validity of our ISP determination.

We employed a similar technique to determine the ISP for π Aqr. We first rotated our data by -166.7° to place any small level of residual intrinsic polarization in our low-state data in the Stokes Q’ parameter and isolating the perpendicular ISP component in the Stokes U’ parameter. We were able to obtain a good fit of a modified Serkowski

law to the co-added U’ data again using *mpcurvefit*, as demonstrated in Figure 9, which plots π Aqr’s U’ component binned to a constant (Poisson photon statistic) polarization error of 0.01%. We do note that a small fraction of the binned U’ data at the extrema of our wavelength coverage, e.g. below $\sim 4000\text{\AA}$ and above $\sim 9500\text{\AA}$, deviate from the best fit by $\leq 0.1\%$. These deviations are less than $3\text{-}\sigma$ from the known instrumental systematic uncertainties (Section 2); hence, we do not believe they represent real features. To confirm this, we also fit the data with an error weighted modified Serkowski-law, after adopting the known systematic instrumental uncertainties for the U- and I-band data, which were larger than the Poisson photon statistic errors. Similar to the result achieved for completely excluding the U- and I-band data from the fit, we found this exercise did not appreciably affect the resultant best fit ISP parameters. Since the number of binned data points which deviate from the fit is extremely small, relative to the total number of binned data points used the fit, these two modifications to the fitting routine had no effect on the resultant best fit. The Serkowski law parameters of π Aqr’s perpendicular ISP component are listed in Table 5.

For the parallel ISP component, we included an additional constant term in our modified Serkowski law fitting, “C”, to accommodate the possibility that a small level of intrinsic polarization was present in our low state data and fixed the value of λ_{max} to that found in the perpendicular ISP component (Table 5), as this parameter should be the same for both the perpendicular and parallel ISP components. The resultant best fit to the Q’ component agrees reasonably well with the data, as seen in Figure 9, with small deviations present below $\sim 4000\text{\AA}$ and above $\sim 9500\text{\AA}$. These $\leq 0.05\%$ deviations from the best fit are less than $3\text{-}\sigma$ from the known instrumental systematic uncertainties (Section 2); hence, we do not believe they are real and, as for the perpendicular ISP fit, they do not significantly influence the best fit parallel ISP parameters. We find the total ISP for π Aqr to be characterized by $P_{max} = 0.514\% \pm 0.001\%$, $\lambda_{max} = 4959 \pm 15\text{\AA}$, PA = 108.7° , and K = 0.83, as computed by vectorally adding the parallel and perpendicular ISP components listed in Table 5. The wavelength dependence of our polarization low state π Aqr data after subtraction of this total ISP, seen in Figure 10 binned to a constant polarization error of 0.005%, exhibits only a small amount of residual polarization ($< 0.1\%$) in either the Stokes Q or U components and exhibits little structure outside of the aforementioned regions in which the HPOL CCD sensitivity is low.

3.3.4. Comparison to Previous ISP Estimates

While we are not aware of any successful attempts to characterize the ISP along the line of sight to 60 Cyg (see e.g. Poeckert et al. 1979), two groups of authors have attempted to derive the ISP along the line of sight to π Aqr. McLean & Clarke (1979) estimated the ISP to be $P_{ism} \sim 0.45\%$ and $\theta_{ism} \sim 130^\circ$ from analysis of field stars, $P_{ism} \geq 0.6\%$ based upon π Aqr’s E(B-V) excess, and $P_{ism} \leq 0.4\%$ and $\theta_{ism} \leq 130^\circ$ from studying the wavelength dependence of broad-band observations. The authors also note that the latter parameters were supported by H α and H β line polarimetry. From these various meth-

ods, McLean & Clarke (1979) adopted the final ISP values of $P_{max} \sim 0.36\%$, $\lambda_{max} = 5400\text{\AA}$, $\theta_{ism} = 120^\circ$, and placed no formal errors on these estimates. Poeckert et al. (1979) analyzed a heterogeneous mix of optical intermediate-band filter polarimetry, H α polarimetry, and IR polarimetry to derive three different ISP estimates with large reduced χ^2 values ranging from 5.6-10.7. While the λ_{max} value derived by Poeckert et al. (1979) agrees with the value we have derived (Table 5) their PA and P_{max} values differ by $\sim 7^\circ$ and up to 0.1% respectively.

4. DISCUSSION

4.1. Disk-Loss and Disk-Renewal Time-scales

Identifying the mechanisms responsible for the disk-loss and disk-renewal phases of classical Be stars (i.e. the transition to and from a “Be” phase and a normal B-star phase) can be aided by an examination of the time-scale of some or all of the four main phases involved: the disk growth phase, the steady-state disk phase, the disk-loss phase, and the steady-state quiescent (diskless) phase.

Our data poorly constrain the time-scale for the complete regeneration of an active disk state from a quiescent diskless state. Owing to the poor temporal sampling of our 60 Cyg data between 1992 and 1997 (Figure 1), we can only place an upper limit on the regeneration of the active disk state observed in our data of < 5 years. We do see evidence of temporary, correlated enhancements in both the V-band polarization and H α EW during 60 Cyg’s quiescent, diskless state, including one moderate event which occurred between June and September 2004 in the V-band polarization data. Similarly, our long-term observations of π Aqr do not cover a full disk regeneration cycle which would enable us to constrain this time-scale. However, we do observe one major, correlated enhancement in both the V-band polarization and H α EW during the quiescent phase (Figure 2), again during the June - September 2004 time-frame in the V-band polarization data. The sparse temporal sampling of 60 Cyg’s and π Aqr’s outburst episodes during their quiescent phases only enables us to place upper limits on the time-scales of their duration of $<$ a few months.

H α monitoring of the B3 star μ Cen, revealed similar types of outburst events occurring during the star’s quiescent phase, which Hanuschik et al. (1993) interpreted as evidence of individual blobs of material being injected into the star’s inner circumstellar environment on time-scales of 2-5 days, and then viscously accreting back onto the star and/or decaying on time-scales of 20-80 days. Given the similarity in time-scales between μ Cen’s quiescent-state H α outburst events and the duration of the polarization component of quiescent state outbursts observed in 60 Cyg and π Aqr, we propose that our data might be diagnosing one (or several) injection events which subsequently viscously dissipate, perhaps arising from the same type of non-radial pulsation events thought to drive the injection events on μ Cen (Rivinius et al. 1998). Such an interpretation is consistent with previous suggestions of non-radial pulsations in both π Aqr (Peters & Gies 2005) and 60 Cyg (Koubsky et al. 2000).

As discussed in Sections 3.1.1 and 3.1.2, our data provide excellent temporal coverage of the disk-loss events of both 60 Cyg and π Aqr. 60 Cyg experienced a gen-

erally monotonic reduction in H α emission strength from its maximum to minimum state over a time-scale of ~ 870 days. We interpret the ~ 120 day lag of the maximum in the H α EW from the maximum V-band polarization as evidence that the disk cleared in an “inside-out” manner. The total dissipation time-scale of 60 Cyg’s disk, e.g. from the maximum polarization level to the minimum H α EW level, of ~ 1000 days is similar to that observed for the dissipation of omicron And’s disk (~ 700 days; Clark et al. 2003). Clark et al. (2003) noted that omicron And’s disk dissipation was consistent with the expected viscous time-scale of the disk, assuming the viscosity parameter α (Shakura & Syunyaev 1973) is ~ 0.1 . Assuming that 60 Cyg’s disk also dissipated on a viscous time-scale, we can derive the viscosity parameter α using equation 19 of Bjorkman & Carciofi (2005):

$$t_{diffusion} = (0.2yr/\alpha) * (r/R_*)^{0.5} \quad (5)$$

. Assuming that the bulk of the scattering events producing the observed polarization occurs at a radial distance of $\sim 2.5 R_*$ (Carciofi et al. 2009) and a ~ 800 day time-scale for the polarization to transform from maximum to minimum state (see Figure 1), we derive a viscosity parameter of ~ 0.14 for 60 Cyg, which is similar to that found for omicron And. By contrast, the loss of π Aqr’s disk as measured by its H α EW proceeded a factor of at least 2.4 times slower (e.g. ~ 2440 days) than 60 Cyg’s disk loss, and Figure 2 clearly illustrates the presence of two extended (~ 390 day and ~ 730 day) outburst events which temporarily stalled the long-term disk loss event. Like 60 Cyg, π Aqr also exhibited a lag between onset of the low-state of the V-band polarization and the low-state of the H α EW, indicating the disk cleared in an “inside-out” manner. The exquisite temporal sampling of our π Aqr data suggests that temporary increases in the mass injection rate into the inner disk may produce substantial deviations from a monotonic, viscous dissipation of Be disks. We therefore suggest that claims of inconsistencies in the formation versus dissipation time-scales of disks with a standard viscous disk model based on sparsely sampled data, as made by Vinicius et al. (2006), might be caused by under-sampling the type of short-lived outbursts observed in our π Aqr data.

4.2. Temporal Changes in the Intrinsic Polarization Position Angle

While our total V-band polarization data for both 60 Cyg and π Aqr both clearly followed a linear trend when plotted on a Stokes Q-U diagram (Figures 4 and 5), close inspection of these figures reveals tentative evidence of small-scale deviations in some of the data from each star’s intrinsic polarization position angle, which seems to increase with the strength of the intrinsic polarization component. To quantify this effect, we calculated the absolute value of the error weighted deviance of each data point from the best fit line denoting the star’s intrinsic PA. We plot these values as a function of the magnitude of the intrinsic polarization component for both 60 Cyg (top panel) and π Aqr (bottom panel) in Figure 11, where filled triangles represent polarization low-state data (Tables 1 and 2) and open diamonds represent high-state data.

Several trends are immediately apparent. For both 60 Cyg and π Aqr, the bulk of the data exhibit a $< 6\sigma$ residual

from the bulk value of the intrinsic PA value; moreover, very few data points at low intrinsic polarization levels deviate at the $> 6\sigma$ level. Just 2 of 15 (13%) of 60 Cyg data below an intrinsic polarization level of 0.3% exhibit a $> 6\sigma$ deviation while a mere 4 of 59 (7%) of π Aqr data below an intrinsic polarization level of 0.6% exhibit a $> 6\sigma$ deviation. By contrast, a substantial, statistically significant number of data at larger intrinsic polarization levels exhibit large deviations from the bulk intrinsic PA. 8 of 15 (53%) of 60 Cyg data above an intrinsic polarization level of 0.3% exhibit a $> 6\sigma$ deviation while 15 of 32 (47%) of π Aqr data above an intrinsic polarization level of 0.6% exhibit a $> 6\sigma$ deviation. If these trends are in fact real, they would indicate that disk material has a stronger likelihood to be located slightly above or below the disk midplane when the inner disk density is larger (i.e. when the intrinsic polarization component is larger). For example, the position angle of the π Aqr data point exhibiting a deviance of $\sim 26\sigma$ deviated by 2.43° from the bulk intrinsic PA of the disk of θ_* of 166.7° .

Before continuing our interpretation of this phenomenon, we consider the appropriateness of our choice of a deviance cutoff, above which we believe the data exhibit a bona-fide deviation from the intrinsic polarization PA (e.g. 6σ in Figure 11). Merely setting a threshold deviance value above which everything is considered real could lead to several false discoveries, owing to random variations in the data. The false-discovery rate (FDR) method, developed by Miller et al. (2001) and employed by Hopkins et al. (2002) and Kowalski et al. (2009), allows us a means to quantify the percentage of false positives above our choice of a threshold deviance value. We model the null distribution (random noise) using the deviance values below an intrinsic polarization level of 0.6% for π Aqr and 0.3% for 60 Cyg. Employing the IDL routine in Appendix B of Miller et al. (2001), we determined that setting a threshold to the deviance value of 7.687 for π Aqr predicts a false-discovery rate of 32%. In other words, of the 19 discoveries above a deviance of 7.687 (spanning the entire intrinsic polarization range in Figure 11), no more than 32% are caused by spurious deviations. If we assume that the four discoveries below an intrinsic polarization of 0.6% are in fact false discoveries, this implies that only 2 of the discoveries above 0.6% are false, e.g. 13 of the 15 data points above the 6σ level in the bottom panel of Figure 11 are real. Even in the worst case scenario that the entire 32% of the sample of false discoveries resides in the discoveries we claimed above the 0.6% intrinsic polarization level, a full 68% of this sample would still be real, statistically sound detections of deviations from the bulk polarization position angle. Similarly, for 60 Cyg, a false-discovery rate of $\leq 33\%$ sets the threshold deviance value at ≥ 6.52 ; hence, of the 9 observed values above this deviance level, at most 3 could be false discoveries. Based on this FDR analysis, we conclude most of our claimed deviations from the bulk PA of both 60 Cyg and π Aqr are in fact real.

To further explore the origin of these PA deviations, we examine the deviance values computed for Figure 11 as a function of time and compare the trends in these data to the temporal evolution of the V-band polarization. Several clear trends are seen in the data for π Aqr (Figure 12):

1) a substantial number of deviance values exceeding the 6σ level coincided with the latter-portion of the ~ 390 day polarimetric outburst noted in Section 3.2.2; and 2) there was no corresponding increase in the PA deviance coinciding with the ~ 730 day polarimetric outburst reported in Section 3.2.2. Inspection of the right panel of Figure 12, which depicts the behavior of the PA deviance during the ~ 390 day outburst, reveals tentative evidence of two separate components in the deviance. The rise of the first component of the deviance outburst (points A to B; Figure 12) spanned < 54 days while the decline of this first component (points B to C; Figure 12) spanned < 13 days. The time-scale of the second component exhibited similarities, with a rise time (points D to E; Figure 12) of < 35 days and a decline time (points E to F; Figure 12) of < 10 days. We note that the frequency of our observations do not trace the decline phase at a sufficient sampling rate to diagnose the precise time-scale of the decline; rather, the time-scales we quote are merely upper limits. We can not exclude the possibility that the PA deviations returned to normal faster than the 10-13 days we quote.

A similar trend is observed in the temporal evolution of the PA deviance of the 60 Cyg data (see Figure 13). A large outburst is seen in the deviance which coincides with the epoch of the single polarimetric outburst noted in Section 3.2.1. Although the sampling of our 60 Cyg polarimetry is much more coarse compared to π Aqr, Figure 13 illustrates that the < 26 -day rise of the deviance outburst (points A to B) and subsequent < 14 -day decline (points B to C) qualitatively matches the rise and decline time-scales observed for π Aqr.

4.2.1. PA Changes: Evidence of Structure in the Inner Disk or Blob Injections?

Variability in the intrinsic polarization position angles of classical Be stars is not typically expected for a standard axisymmetric disk system, although short-term (Carciofi et al. 2007) and long-term (Carciofi et al. 2007; Tanaka et al. 2007) changes have been reported. Carciofi et al. (2007) attributed variability on time-scales of hours to weeks in the Achernar system as evidence of the injection of blobs into the inner disk, leading to changes in the observed level of polarization and small changes in the polarization position angle which persist on order several weeks until the blob is circularized into a ring. By contrast, Tanaka et al. (2007) attribute the decade time-scale evolution of Pleione's intrinsic polarization PA to disk precession caused by the system's binary companion. We interpret the short-term variability (tens of days) of the intrinsic polarization position angle of both π Aqr and 60 Cyg as evidence of low-amplitude, temporary departures from a simple axisymmetric disk density within the inner disk regions (several stellar radii) of these systems.

The deviations from axisymmetry we observe could be diagnostics of the injection of new blobs into the inner disk region, which subsequently circularize into a ring, thereby acting as an effective warp of the inner disk (see e.g. Figure 14). Carciofi et al. (2007) reported variability in the polarization magnitude and position angle of the Be star Achernar, and offered a similar interpretation. These authors noted that the circularization of a single blob would occur on time-scales of days and that the time-scale for

a ring to incorporate into the inner disk region would be several weeks. The newly injected material would then be re-accreted onto the central star if the mass-loss episode was a singular event, whereas a steady stream of mass-loss episodes would cause the disk size and density to grow over time (Carciofi et al. 2007). As the PA variations in the events observed in both π Aqr and 60 Cyg grew over time-scales of 1-2 months and decayed in \leq 1-2 weeks, we speculate that perhaps the departure from axi-symmetry we witnessed was caused by the injection of multiple blobs into these systems which circularized into a ring and were later incorporated into the inner disk region.

Alternatively, the observed deviations from axisymmetry could be caused by a blob or series of blobs launched from a non-equatorial latitude from the stellar photosphere (Figure 14). Such blob(s) would still circularize on time-scales of days to weeks, but owing to the latitude of their ejection they would circularize into an inclined (non-coplanar) orbit with respect to the sem-major axis of the bulk of the disk material. One could imagine this inclined ring eventually incorporating itself into the plane of the bulk of the disk material owing to viscous drag (or other) forces. Thus we speculate that perhaps our observation of a temporary deviation in the polarization position angle might be diagnosing the presence of a newly injected blob, which is subsequently circularized, at an inclined orbit with respect to the plane of the pre-existing disk material. We plan to explore the feasibility of both of the above scenarios using models similar to those presented in Carciofi et al. (2007) in a future publication.

We note that one of the polarimetric outbursts of π Aqr, occurring in 1994 June, was not accompanied by a corresponding variation in the polarization position angle (see e.g. Figure 12). Unlike the other outbursts, our temporal coverage of the 1994 event was especially sparse. π Aqr’s V-band polarization was elevated in observations obtained on 5 June 1994, 7 June 1994, and 22 June 1994. However, the onset of this outburst is unknown, as no observations were obtained between 10 September 1993 and the elevated 5 June 1994 observation. Similarly, there was a \sim 6 week gap between the last elevated observation on 22 June 1994 and the subsequent observation on 3 August 1994, which merely places an upper limit on the time-scale of the polarization decline (of $<$ 6 weeks). Given this sparse data sampling, we speculate that it is possible that we simply “missed” observing the injection events which would have produced variations in the PA, and instead only sampled the aftermath of these events in which newly injected material had already circularized in the disk. Alternatively, it is also possible that not all mass injection events yield deviations from axi-symmetry. Clearly, additional observations of more polarimetric outburst events, at a higher sampling frequency, are needed to better constrain this phenomenon.

4.3. Long-term Disk Loss/Disk Renewal Behavior of 60 Cyg

While our long-term Lyot and HPOL polarimetric monitoring of π Aqr only covered 1 complete cycle of a Be to normal-B transition, our polarimetric observations of 60 Cyg actually span multiple disk loss/disk renewal transitions. Specifically, there is clear evidence from the long-

term behavior of both the V-band polarization and H- α EW (see Figure 1; also Koubsky et al. 2000) that the circumstellar disk diagnosed by our 1987 PBO Lyot polarimetric observation had dissipated by the early 1990s and that our polarimetric data from 1997-2000 was probing a physically new circumstellar disk. Interestingly, after subtracting the ISP from both the PBO Lyot and PBO HPOL polarimetry, we find the exact same (intrinsic) polarization position angle in both data sets. This indicates that the older (late 1980s) and most recently generated (1997-2000) disks shared the same equatorial plane on the sky, and suggests a similar formation mechanism was responsible for both events. We note that this scenario is fundamentally different than the misaligned double-disk structure reported for Pleione by Tanaka et al. (2007), whereby the authors suggested that the PA of the disk was precessing due to interactions with the star’s binary companion.

5. FUTURE WORK

We have shown that the relatively rare occurrence of a disk-loss episode in classical Be stars provides a unique opportunity to constrain the interstellar polarization component along the line of sight to these stars in exquisite detail. While we have analyzed the behavior of the total polarization of our dataset, our accurate ISP determination will facilitate the improved removal of the interstellar component and thereby enable the time evolution of the intrinsic polarization component of these data to be studied in detail. We are currently analyzing the behavior of the intrinsic polarization of these stars and plan to present results of detailed modeling of these systems, using the Monte Carlo code of Carciofi & Bjorkman (2006), in a future publication.

We also encourage observers to follow-up on the results presented in Section 4.2, which indicate that the polarization PA of classical Be star disks may exhibit small-scale deviations during polarization outbursts. We have suggested that the origin of these deviations might be evidence of newly injected blobs in the disk which have not yet circularized into a ring, or evidence of new blobs which were launched from a non-equatorial latitude thereby projecting them into an inclined circular orbit with respect to the plane of the pre-existing disk material. We encourage high time cadence observations which diagnose the inner regions of such disk systems, such as polarimetry and/or infrared spectroscopy, to further constrain the origin of this phenomenon.

6. SUMMARY

We have presented the results of 127 spectropolarimetric observations of the Be star π Aqr spanning 15 years, and 35 spectropolarimetric and 65 H α spectroscopic observations of the Be star 60 Cyg spanning 14 years. These data trace the evolution of each star as it transitions from having a gaseous circumstellar disk (“Be phase”) to a diskless state (“normal B-star phase”). We find:

- 60 Cyg’s disk emission strength, as measured by its H α EW, declined from maximum emission to pure absorption monotonically in \sim 870 days. The maximum observed H α EW lagged the maximum observed V-band polarization by \sim 120 days, indicating

that the total disk dissipation time-scale was ~ 1000 days ($\sim 870 + \sim 120$), and that the disk clearing proceeded in an “inside-out” fashion. We found the dissipation of disk, as measured from the time-scale of the decrease in the observed polarization, occurred over a viscous time-scale if we adopted a viscosity parameter α of 0.14.

- π Aqr’s disk emission strength as measured by its H α EW declined from maximum emission to pure absorption over a time-frame of ~ 2440 days. Two extended outburst events lasting ~ 390 and ~ 730 days respectively were observed during π Aqr’s diskless phase, which had the effect of temporarily stalling the loss of the disk. An observed lag in the onset of the minimum H α EW strength from the minimum V-band polarization indicates that π Aqr’s disk clearing also proceeded in an “inside-out” fashion.
- The time-scale of the disk-loss events in 60 Cyg and π Aqr corresponds to almost 6 and 29 complete orbits of each star’s binary companion respectively. This suggests that each star’s binary companion does not influence the primary star (or its disk) in a manner similar to the highly eccentric δ Sco system (Miroshnichenko et al. 2001).
- We fit the wavelength dependence of multi-epoch spectropolarimetric observations obtained during the quiescent diskless phase of each star with a modified Serkowski law to derive the interstellar polarization along the line of sight to each star. We determine the best fit modified Serkowski law parameters for 60 Cyg to be $P_{max} = 0.112\% \pm 0.001\%$, $\lambda_{max} = 6977\text{\AA}$, PA = 41.5° , and K = 1.17, while for π Aqr we derive the parameters $P_{max} = 0.514\% \pm 0.001\%$, $\lambda_{max} = 4959\text{\AA}$, PA = 108.7° , and K = 0.83.
- We find that the position angle of intrinsic polarization arising from 60 Cyg’s disk is $\theta_* = 107.7 \pm 0.4^\circ$, indicating that the disk is oriented on the sky at a position angle of $\theta_{disk} = 17.7^\circ$ (measured North to East). We find that the position angle of intrinsic polarization arising from π Aqr’s disk is $\theta_* = 166.7 \pm 0.1^\circ$, indicating that the disk is oriented on the sky at a position angle of $\theta_{disk} = 76.7^\circ$.
- We detect clear evidence of small outburst events in the V-band polarization and H α EW during the quiescent diskless phase of both π Aqr and 60

Cyg, which persist for several months in the V-band polarization. As these events have similar time-scales as the blob injection events likely induced by non-radial pulsations in the Be star μ Cen (Hanuschik et al. 1993; Rivinius et al. 1998), we suggest these outburst events indicate the injection of one (or several) blobs of material from the stellar photosphere which are subsequently accreted back onto the central star and/or decreted on a viscous time-scale.

- We also detect evidence of deviations from the intrinsic polarization position angle in both 60 Cyg and π Aqr which persist for 1-2 months and coincide with large outbursts in the total V-band polarization, and confirm these events are real via an examination of the false discovery rate for each object. For π Aqr, we determine the magnitude of one of these deviations to be $\sim 2.43^\circ$ from the bulk intrinsic polarization PA of the disk (166.7°). These results are indicative of deviations from a simple axisymmetric disk density structure in each system. We propose that either we are witnessing the injection and subsequent circularization of new blobs into the inner disk region in a similar manner as noted by Carciofi et al. (2007) or the injection and subsequent circularization of new blobs at an inclined orbit to the plane of pre-existing disk material (see Figure 14).

We thank our referee, David Harrington, for providing helpful suggestions which improved the quality of this paper. We also thank Brian Babler for his invaluable assistance with various aspects of PBO HPOL data, the PBO and Ritter science teams for providing observing and data reduction support, and Kenneth H. Nordisiek for providing access to the PBO Lyot and HPOL spectropolarimeters. JPW thanks A. Carciofi and A. Okazaki for providing helpful comments regarding the effects of binary companions in Be star systems. JPW acknowledges support from NSF Astronomy & Astrophysics Postdoctoral Fellowship AST 08-02230, and ZHD acknowledges partial support from the University of Washington Pre-MAP program. HPOL observations were supported under NASA contract NAS5-26777 with the University of Wisconsin-Madison. Observations at the Ritter Observatory are supported by the NSF under the PREST grant AST 04-40784. This study has made use of the SIMBAD database, operated at CDS, Strasbourg, France, and the NASA ADS service.

REFERENCES

- Bjorkman, J. E., & Cassinelli, J. P. 1993, ApJ, 409, 429
 Bjorkman, K.S. et al. 1998, ApJ, 509, 904
 Bjorkman, K.S., Miroshnichenko, A.S., McDavid, D., & Pogrosheva, T.M. 2002, ApJ, 573, 812
 Bjorkman, J.E. & Carciofi, A.C. 2005, in ASP Conf Ser. 337, The Nature and Evolution of Disks Around Hot Stars, ed R. Ignace & K. Gayley (San Francisco: ASP), 75
 Brown, J.C., Cassinelli, J.C., & Maheswaran, M. 2008, ApJ, 688, 1320
 Carciofi, A.C. & Bjorkman, J.E. 2006, ApJ, 639, 1081
 Carciofi, A.C., Magalhaes, A.M., Leister, N.V., Bjorkman, J.E., & Levenhagen, R.S. 2007, ApJL, 671, 49
 Carciofi, A.C., Okazaki, A.T., le Bouquin, J.-B., Steff, S., Rivinius, Th., Baade, D., Bjorkman, J., & Hummel, C.A. 2009, A&A, 504, 915
 Cassinelli, J.P., Brown, J.C., Maheswaran, M., Miller, N.A., & Telfer, D.C. 2002, ApJ, 578, 951
 Chalabaev, A. & Maillard, J.P. 1983, A&A, 127, 279
 Clark, J.S., Tarasov, A.E., & Panko, E.A. 2003, A&A, 403, 239
 Clarke, D. & Bjorkman, K.S. 1998, A&A, 331, 1059
 Coyne, G.V. & Kruszewski, A. 1969, AJ, 74, 528
 Cranmer, S.R. 2005, ApJ, 634, 585
 Cranmer, S.R. 2009, ApJ, 701, 396

- Doazan, V., Franco, M., Rusconi, L., Sedmak, G., & Stalio, R. 1983, *A&A*, 128, 171
- Eggleton, P.P. 1983, *ApJ*, 268, 368
- Hanuschik, R.W., Dachs, J., Baudzus, M., & Thimm, G. 1993, *A&A*, 274, 356
- Harries, T.J., Babler, B.L., & Fox, G.K. 2000, *A&A*, 361, 273
- Harrington, J.P. & Collins, G.W. 1968, *ApJ*, 151, 1051
- Harrington, D.M. & Kuhn, J.R. 2009, *ApJS*, 180, 138
- Heiles, C. 2000, *AJ*, 119, 923
- Hopkins, A.M., Miller, C.J., Connolly, A.J., Genovese, C., Nichol, R.C., & Wasserman, L. 2002, *AJ*, 123, 1086
- Koubsky, P. et al 2000, *A&A*, 356, 913
- Kowalski, A.F., Hawley, S.L., Hilton, E.J., Becker, A.C., West, A.A., Bochanski, J.J., & Sesar, B. 2009, *AJ*, 138, 633
- Lee, U., Osaki, Y., & Saio, H. 1991, *MNRAS*, 250, 432
- Lupie, O.L. & Nordsieck, K.H. 1987, *AJ*, 93, 214
- Mathewson, D. S., & Ford, V. L. 1970, *Mem.R.A.S.*, 74, 139
- McDavid, D. 1986, *PASP*, 98, 572
- McDavid, D. 1990, *PASP*, 102, 773
- McDavid, D. 1994, *PASP*, 106, 949
- McDavid, D. 1999, *PASP*, 111, 494
- McLean, I. S., & Brown, J. C. 1978, *A&A*, 69, 291
- McLean, I. S., & Clarke, D. 1979, *MNRAS*, 186, 245
- McSwain, M.V., Huang, W., & Gies, D.R. 2009, *ApJ*, 700, 1216
- Meyer, J.M., Nordsieck, K.H., & Hoffman, J.L. 2002, *AJ*, 123, 1639
- Miller, C.J. et al. 2001, *AJ*, 122, 3492
- Miroshnichenko, A.S. et al. 2001, *A&A*, 377, 485
- Morrison, N.D., Knauth, D.C., Mulliss, C.L., & Lee, W. 1997, *PASP*, 109, 676
- Neiner, C. 2002, *A&A*, 388, 899
- Nook, M. 1990, Ph.D. dissertation, The University of Wisconsin-Madison
- Nook, M., Cardelli, J.A., & Nordsieck, K.H. 1990, *AJ*, 100, 2004
- Nordsieck, K.H. et al. 2001, in *ASP Conf Ser. 233, P Cygni 2000: 400 Years of Progress*, ed. M. de Groot & C. Sterken (San Francisco: ASP), 261
- Nordsieck, K. H., & Harris, W. 1996, *ASP Conf. Ser. 97, Polarimetry of the Interstellar Medium*, ed. W. G. Roberge & D. C. B. Whittet (San Francisco: ASP), 100
- Okazaki, A.T. 1991, *PASJ*, 43, 75
- Oudmaijer, R.D., Drew, J.E., & Vink, J.S. 2005, *MNRAS*, 364, 725
- Oktariani, F. & Okazaki, A.T. 2009, *PASJ*, 61, 57
- Perryman, M.A.C. et al 1997, *A&A*, 323, 49
- Peters, G.J. & Gies, D.R. 2005, in *ASP Conf Ser. 337, The Nature and Evolution of Disks Around Hot Stars*, ed R. Ignace & K. Gayley (San Francisco: ASP), 294
- Poeckert, R., & Marlborough, J. M. 1978a, *ApJ*, 220, 940
- Poeckert, R. & Marlborough, J.M. 1978b, *ApJS*, 38, 229
- Poeckert, R., Bastien, P., & Landstreet, J. D. 1979, *AJ*, 84, 812
- Poeckert, R., Gulliver, A.F., & Marlborough, J.M. 1982, *PASP*, 94, 87
- Porter, J.M. & Rivinius, T. 2003, *PASP*, 115, 1153
- Quirrenbach, A., Bjorkman, K. S., Bjorkman, J. E., Hummel, C. A., Buscher, D. F., Armstrong, J. T., Mozurkewich, D., Elias, N. M., & Babler, B. L. 1997, *ApJ*, 479, 477
- Rivinius, Th., Baade, D., Stefl, S., Stahl, O., Wolf, B., & Kaufer, A. 1998, *A&A*, 333, 125
- Serkowski, K., Mathewson, D. S., & Ford, V. L. 1975, *ApJ*, 196, 261
- Shakura, N.I. & Syunyaev, R.A. 1973, *A&A*, 24, 337
- Slettebak, A. 1982, *ApJS*, 50, 55
- Steff, S. et al. 2009, *A&A*, 504, 929
- Struve, O. 1931, *ApJ*, 73, 94
- Tanaka, K., Sadakane, K., Narusawa, S., Naito, H., Kambe, E., Katahira, J., & Hirata, R. 2007, *PASJ*, 59, L35
- Townsend, R.H.D., Owocki, S.P., & Howarth, I.D. 2004, *MNRAS*, 350, 189
- Underhill, A. & Doazan, V. eds. 1982, *B Stars with and without Emission Lines* (NASA SP-456; Washington, DC: NASA)
- Vinicius, M.M.F., Zorec, J., Leister, N.V., & Levenhagen, R.S. 2006, *A&A*, 446, 643
- Whitehurst, R. & King, A. 1991, *MNRAS*, 249, 25
- Whitney, B.A. & Clayton, G.C. 1989, *AJ*, 98, 297
- Wilkink, B. A., Lebofsky, M. J., & Rieke, G. H. 1982, *AJ*, 87, 695
- Wisniewski, J.P., Babler, B.L., Bjorkman, K.S., Kurchakov, A.V., Meade, M.R., & Miroshnichenko, A.S. 2006, *PASP*, 118, 820
- Wisniewski, J.P., Kowalski, A.F., Bjorkman, K.S., Bjorkman, J.E., & Carciofi, A.C. 2007a, *ApJL*, 656, 21
- Wisniewski, J.P., Bjorkman, K.S., Magalhaes, A.M., Bjorkman, J.E., Meade, M.R., & Pereyra, A. 2007b, *ApJ*, 671, 2040
- Wolff, M. J., Nordsieck, K. H., & Nook, M. A. 1996, *AJ*, 111, 856
- Wood, K., Bjorkman, J. E., Whitney, B. A., & Code, A. D. 1996a, *ApJ*, 461, 828
- Wood, K., Bjorkman, J. E., Whitney, B. A., & Code, A. D. 1996b, *ApJ*, 461, 847
- Wood, K., Bjorkman, K. S., & Bjorkman, J. E. 1997, *ApJ*, 477, 926

TABLE 1
SUMMARY OF 60 CYG DATA

Date	JD	Obs	H α EW	V-band Pol	PA	State
...	Å	%	degrees	...
1992 Aug 3	2448837	PBO	4.5 ± 0.1	0.074 ± 0.006	58.2	H
1992 Aug 31	2448865	PBO	3.5 ± 0.1	0.108 ± 0.004	52.2	H
1997 Nov 10	2450732	PBO	-5.5 ± 0.1	0.631 ± 0.003	102.1	H

Note. — A sample summary of spectroscopic and spectropolarimetric observations of 60 Cygni; the full version of this Table is available in the online-edition of this Journal. The third column denotes the location at which the data were obtained (PBO = Pine Bluff Observatory, RIT = Ritter Observatory), while the seventh column denotes a qualitative assessment of whether 60 Cyg is in a polarimetrically high state (H), indicative of the presence of a strong disk, or in a polarimetrically low state (L), in which evidence of the presence of a disk is absent (see Section 3.3.3 for further discussion of these designations). Note that we have labeled the two observations in 1992 August as being “high state”, primarily because they are isolated from subsequent observations by ~ 5 years.

TABLE 2
SUMMARY OF π AQR DATA

Date	JD	Obs	H α EW	V-band Pol	PA	State
...	Å	%	degrees	...
1985 May 15	2446200	McD ¹	...	1.53±0.03	158.8	...
1986 Jun 15	2446596	McD ²	...	1.47±0.02	159.1	...
1987 Aug 15	2447022	McD ²	...	1.50±0.03	157.4	...
1988 Jul 15	2447357	McD ²	...	1.04±0.06	155.0	...
1989 Jun 15	2447692	McD ²	...	0.97±0.04	152.1	...
1989 Aug 8	2447747	PBO	-23.5±0.1	1.277±0.005	156.5	H
1989 Oct 26	2447826	PBO	-24.6±0.1	0.879±0.003	148.9	H

Note. — A sample summary of spectroscopic and spectropolarimetric observations of π Aquarii; the full version of this Table is available in the online-edition of this Journal. The third column denotes the location at which the data were obtained (PBO = Pine Bluff Observatory, McD = McDonald Observatory), while the seventh column denotes a qualitative assessment of whether π Aqr is in a polarimetrically high state (H), indicative of the presence of a strong disk, or in a polarimetrically low state (L), in which evidence of the presence of a disk is absent (see Section 3.3.3 for further discussion of these designations). ¹ data are from McDavid (1986), ² data are from McDavid (1990).

TABLE 3
PBO LYOT POLARIMETRY

Target Star ...	JD ...	Date ...	%Pol. %	P.A. degrees	Wavelength Coverage Å
60 Cyg	2446998	1987 Jul 22	0.44 ± 0.02	104	4600-7200
π Aqr	2444116	1979 Aug 31	1.17 ± 0.03	153	4800-7600
π Aqr	2444131	1979 Sep 15	1.13 ± 0.02	155	4800-7600
π Aqr	2444133	1979 Sep 17	1.16 ± 0.03	156	4800-7600
π Aqr	2444138	1979 Sept 22	1.12 ± 0.02	157	4800-7600
π Aqr	2444439	1980 Jul 19	1.31 ± 0.12	159	4800-8200

Note. — Summary of polarization measurements of 60 Cyg and π Aqr obtained between 1979-1987 using the Lyot Polarimeter at the University of Wisconsin's Pine Bluff Observatory 36" telescope.

TABLE 4
FIELD STAR POLARIZATION DATA

Target Star	Field Star	Spectral Type	Distance(pc)	%Pol.	P.A.
π Aqr	HD213789	G6III	136	0.53 ¹	133.7 ¹
π Aqr	HD213119	K5III	178	0.23 ¹	110.4 ¹
π Aqr	HD212320	G6III	141	0.44 ¹	160.5 ¹
π Aqr	HD211924	B5IV	282	1.16 ¹	140.2 ¹
π Aqr	HD211838	B8III	228	0.46 ¹	138.8 ¹
π Aqr	HD211304	B9	306	0.22 ¹	107.6 ¹
π Aqr	HD211099	B9	455	0.26 ¹	119.2 ¹
60 Cyg	HD198915	B6V	288	0.19 ²	15.0 ²

Note. — Note that spectral types were obtained from SIMBAD, and distance measurements were obtained from the Hipparcos catalog (Perryman et al. 1997). For reference, the Hipparcos derived distances to π Aqr and 60 Cyg are 340pc and 418pc respectively. Archival polarization data were compiled from ¹Mathewson & Ford (1970) and ²Heiles (2000).

TABLE 5
SUMMARY OF INTERSTELLAR POLARIZATION VALUES

Star	Value	P_{max}	λ_{max}	PA	K	C
60 Cyg	Q'	-0.076 ± 0.000	6977 ± 241	135.0	1.17	0
60 Cyg	U'	-0.083 ± 0.001	6977 ± 241	90.0	1.17	0
60 Cyg	P	0.112 ± 0.001	6977 ± 241	41.5	1.17	0
Pi Aqr	Q'	-0.265 ± 0.001	4959 ± 15	135.0	0.83	0.04
Pi Aqr	U'	-0.462 ± 0.001	4959 ± 15	90.0	0.83	0
Pi Aqr	P	0.514 ± 0.001	4959 ± 15	108.7	0.83	0

Note. — The derived modified Serkowski law parameters (Serkowski et al. 1975; Wilking et al. 1982) derived for the perpendicular (U') and parallel (Q') ISP components. The total ISP estimate for each star was computed by vectorial addition of the quoted parallel and perpendicular components. Note that column 7, “C”, denotes a constant term added to the modified Serkowski-law fit of the π Aqr parallel ISP component to accommodate the presence of a possible small intrinsic polarization component.

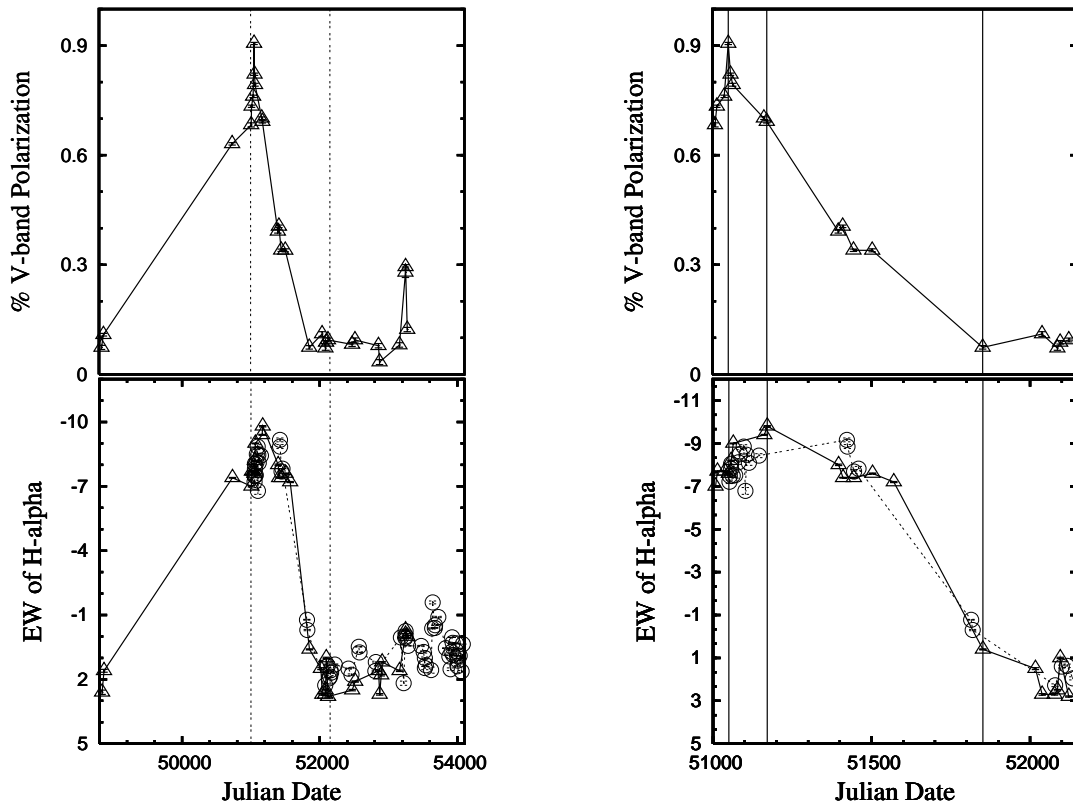


FIG. 1.— The time evolution of 60 Cyg’s observed (intrinsic and ISP) V-band polarization (top panels) and H α EW (bottom panels) is illustrated for our entire dataset (left figure set) and a zoomed region (right figure set). Open circles correspond to Ritter observations while open triangles correspond to HPOL observations, and error bars (compiled in Table 1) are smaller than the size of the data points. As discussed in Section 2, a factor of -1.9 \AA has been added to HPOL EW data compiled in Table 1. The three vertical lines in the right figure set depict (from left to right) the epoch of the maximum V-band polarization (JD=2451049), the maximum H α EW (JD=2451171), and the minimum H α EW (JD=2452038). The monotonically decreasing H α EW strength demonstrates the gradual loss of 60 Cyg’s disk over a time-scale of ~ 870 days. The ~ 120 day lag of the maximum H α EW from the maximum V-band polarization and the ~ 190 day lag of the onset of the minimum H α EW from the onset of the minimum V-band polarization suggest that the disk-clearing progressed in an “inside-out” manner. The full time-scale for disk loss, from the maximum V-band polarization to the minimum H α EW, is ~ 1000 days (~ 870 days + ~ 120 days).

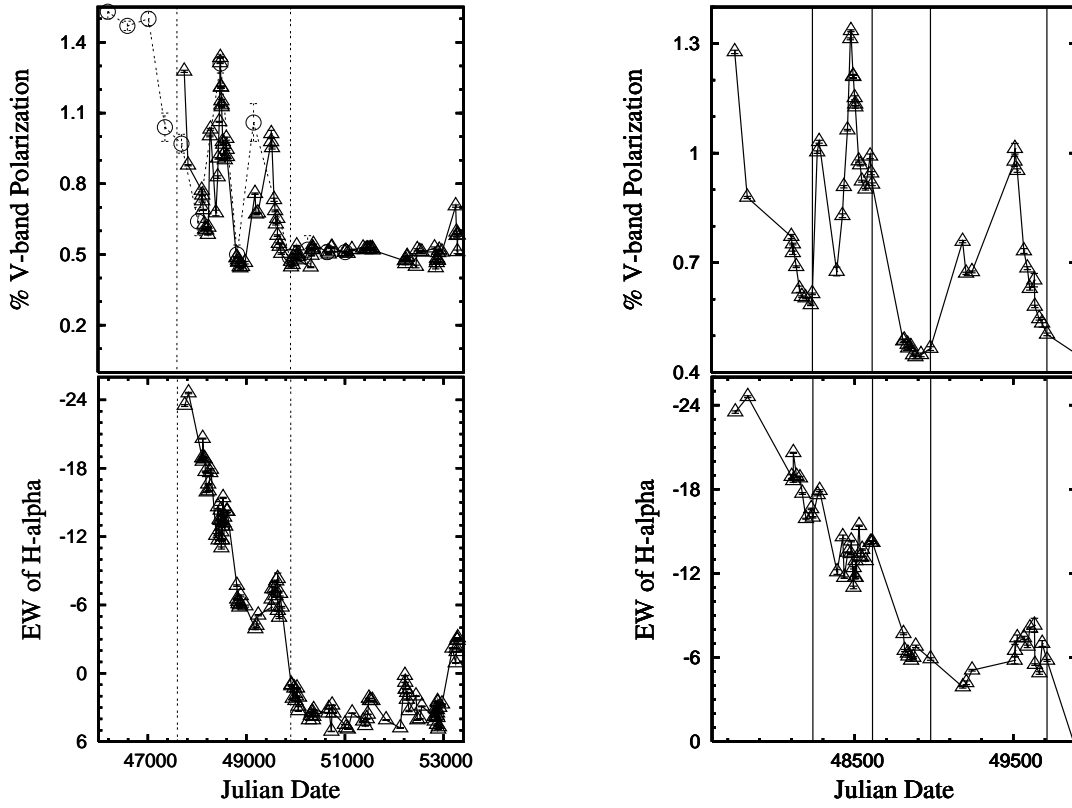


FIG. 2.— The temporal evolution of π Aquarii’s observed (intrinsic and ISP) V-band polarization (top panels) and H α EW (bottom panels) are illustrated for our entire dataset (left figure set) and a zoomed region (right figure set). Open triangles correspond to our HPOL data while open circles correspond to literature V-band polarization values compiled by McDavid (1986, 1990, 1994, 1999). HPOL EW and polarization errors (compiled in Table 2) are smaller than the size of the data points. The vertical lines in the right figure set denote (from left to right) the onset (JD=2448226) and termination (JD=2448612) of the \sim 390 day long first polarimetric outburst and the onset (JD=2448979) and termination (JD=2449713) of the \sim 730 day long second polarimetric outburst.

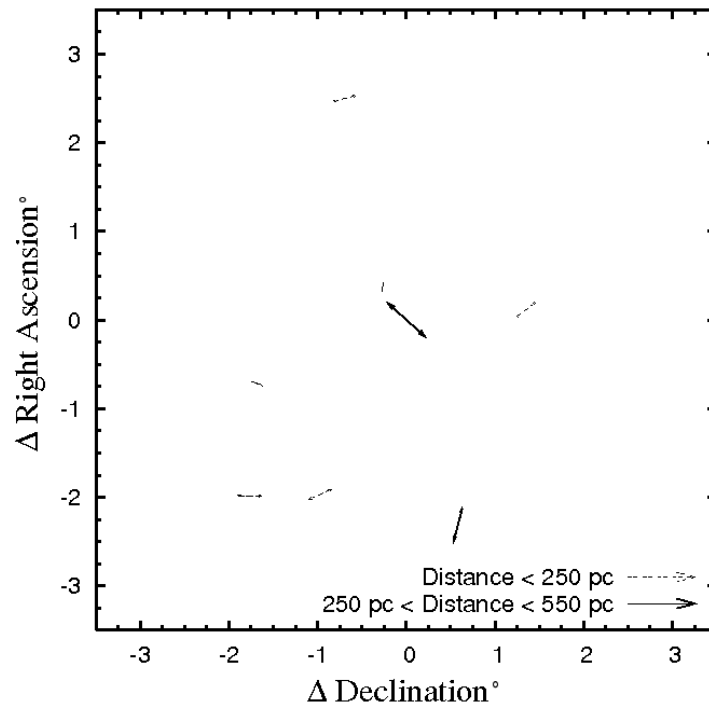


FIG. 3.— The polarization values of stars nearby the location of 60 Cyg, based on the polarization catalog of Heiles (2000). One star having a similar distance (250 - 550 pc) as 60 Cyg (418 pc Perryman et al. 1997), shown with a solid line, exhibits significantly different polarization than 60 Cyg, indicating that a useful ISP estimate along the line of sight to 60 Cyg cannot be obtained from these data. For reference, the length of the vectors in the legend correspond to a polarization magnitude of 0.325%.

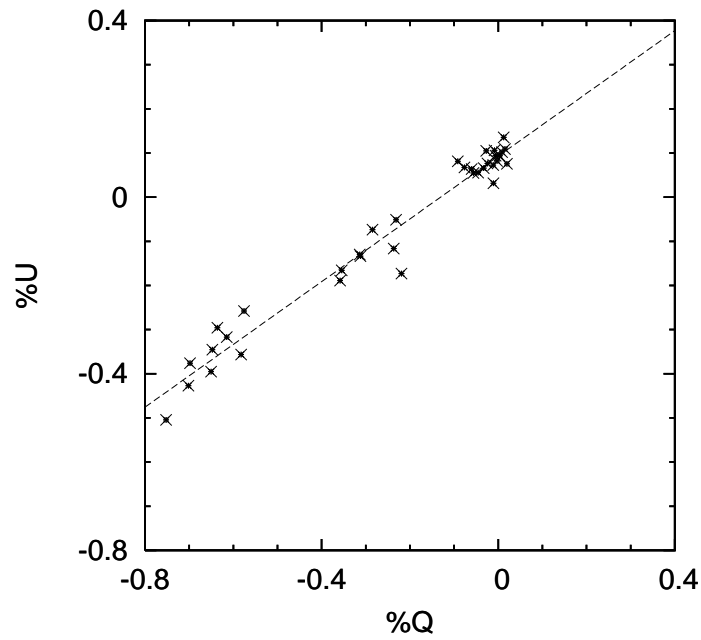


FIG. 4.— The V-band polarization of our entire dataset for 60 Cyg is plotted on a Stokes Q-U diagram. Note that the polarization errors (compiled in Table 1) are smaller than the size of the data points. The data follow a strict linear trend indicating a constant scattering angle (i.e. polarization position angle) as expected in an electron scattering gaseous circumstellar disk system. The slope of the best fit linear regression to the data, 0.71 ± 0.02 , yields the intrinsic polarization position angle of 60 Cyg, $\theta_* = 107.7 \pm 0.4^\circ$. This implies that 60 Cyg's disk is oriented at a position angle of $\theta_{disk} = 17.7^\circ$ on the sky.

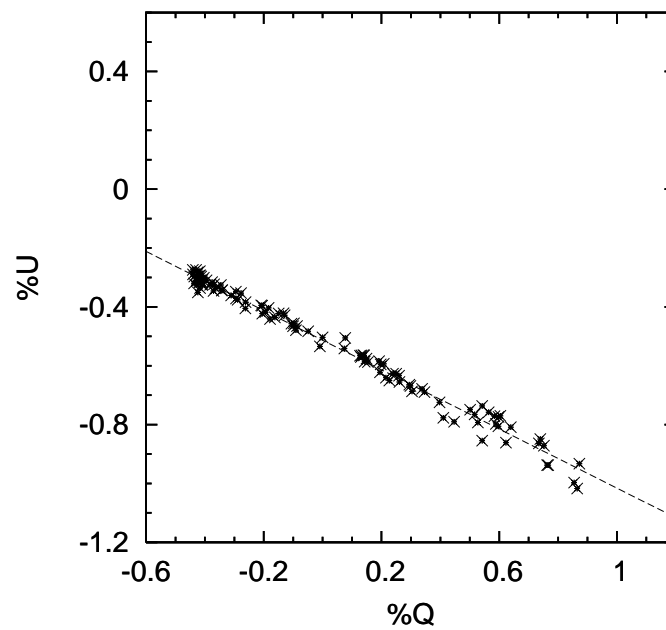


FIG. 5.— The V-band polarization of our entire dataset for π Aqr is plotted on a Stokes Q-U diagram. Note that the polarization errors (compiled in Table 2) are smaller than the size of the data points. Similar to 60 Cyg (Figure 4), the data follow a linear trend indicative of a constant scattering angle as expected in a circumstellar disk system. The slope of the best fit linear regression to the data, -0.50 ± 0.01 , yields the intrinsic polarization position angle of π Aqr, $\theta_* = 166.7 \pm 0.1^\circ$. This implies that π Aqr's disk is oriented at a position angle of $\theta_{disk} = 76.7^\circ$ on the sky.

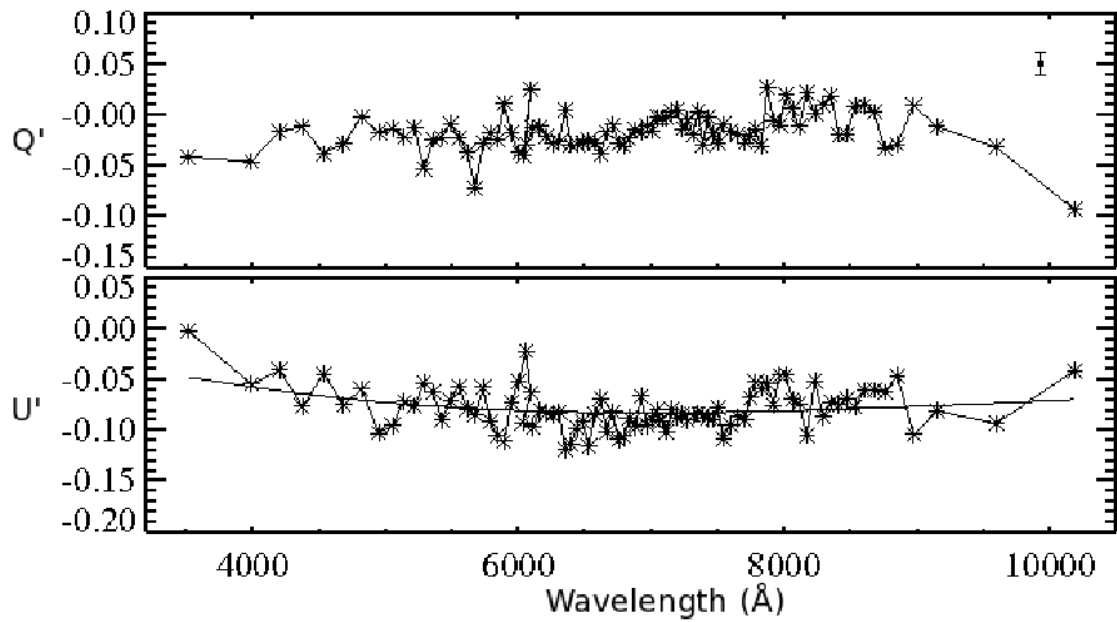


FIG. 6.— The wavelength dependence of 60 Cyg’s polarization low-state data, binned to a constant (Poisson photon statistic) polarization error of 0.01% (depicted as a representative error bar), in the rotated Stokes U' component (see Section 3.3.3) was fit with a modified Serkowski law (Serkowski et al. 1975; Wilking et al. 1982), yielding the estimate of the perpendicular ISP component along the line of sight to the star. The data in the rotated Stokes Q' component, representing the parallel component of the ISP, was close to zero and not well fit by a Serkowski law. Section 3.3.3 provides a discussion of how we estimated the parallel ISP component for 60 Cyg. The parallel, perpendicular, and total ISP values adopted in this paper are summarized in Table 5.

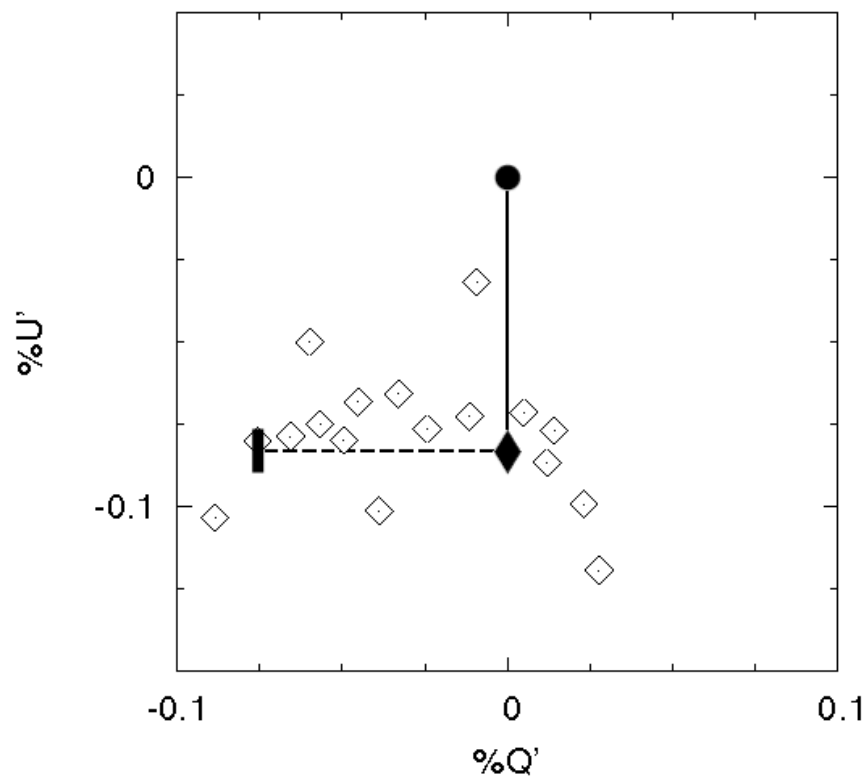


FIG. 7.— The low state (diskless) 60 Cyg V-band polarimetric data are plotted on a Stokes Q' - U' diagram. Errors are smaller than the size of the data points. As discussed in Section 3.3.3 and illustrated in Figure 6, we fit a modified Serkowski law to the U' component of these data to extract the perpendicular component of the interstellar polarization (denoted here by the solid line). Since the wavelength dependence of the U' data were not well represented by a Serkowski law (see Figure 6, we determined the minimum parallel component of the interstellar polarization to be simply the vector along the Q' direction which joined the end of the perpendicular ISP component with the data having the minimum Q' value, (denoted by the dashed line). This minimum parallel ISP component is tabulated in Table 5.

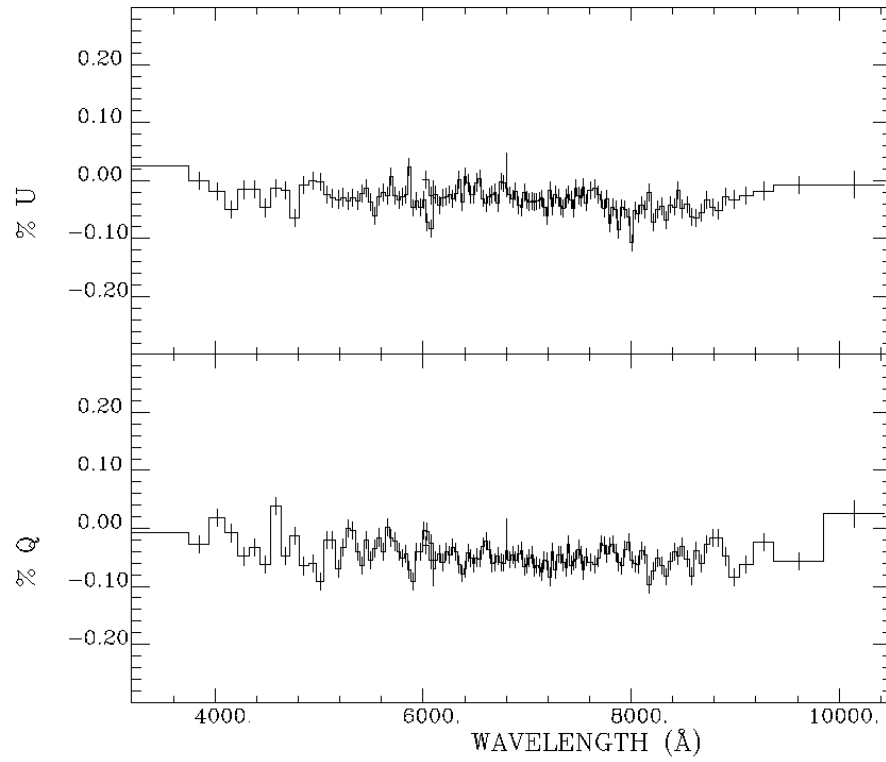


FIG. 8.— The residuals of our low-state 60 Cyg data, binned to a constant (Poisson photon statistic) polarization error of 0.015%, are shown after subtracting the total ISP values listed in Table 5. The data are consistent with $Q = 0\%$ and $U = 0\%$ and exhibit no significant wavelength dependence, providing confidence in the total interstellar polarization values we derived for 60 Cyg.

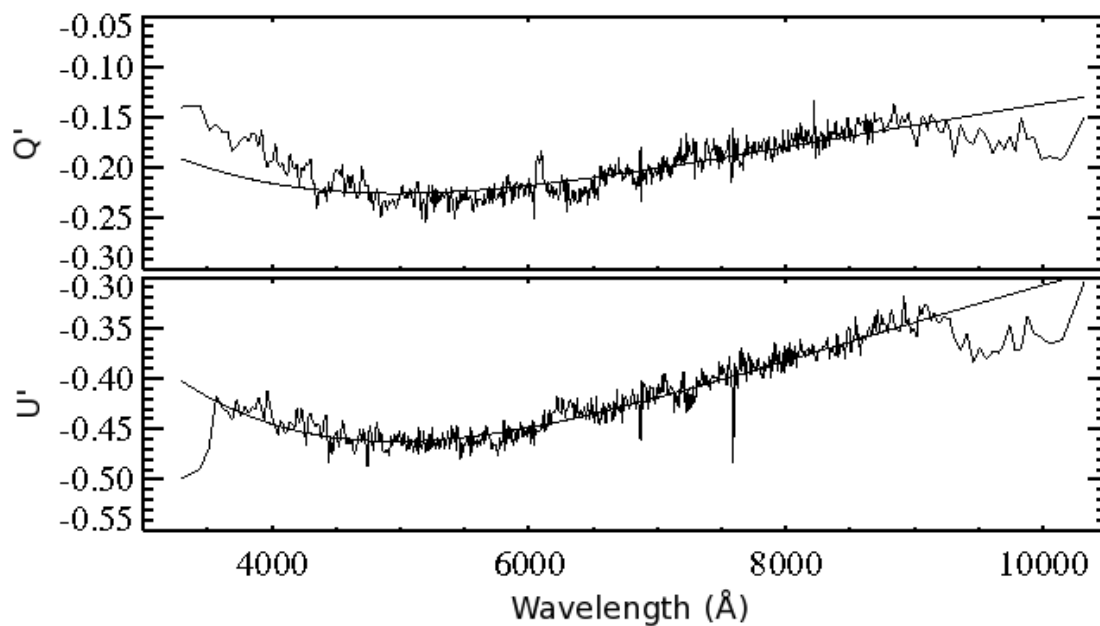


FIG. 9.— The wavelength dependence of π Aqr’s polarization low-state data, binned to a constant (Poisson photon statistic) polarization error of 0.01%, in the rotated Stokes U' component (see Section 3.3.3) was fit with a modified Serkowski law (Serkowski et al. 1975; Wilking et al. 1982), yielding the estimate of the perpendicular ISP component along the line of sight to the star (shown). The data in the rotated Stokes Q' component, representing the parallel component of the ISP, were also fit with a modified Serkowski law (shown), which included an additional constant term to account for the presence of a potential remnant intrinsic polarization component. The parallel, perpendicular, and total ISP values adopted in this paper are summarized in Table 5.

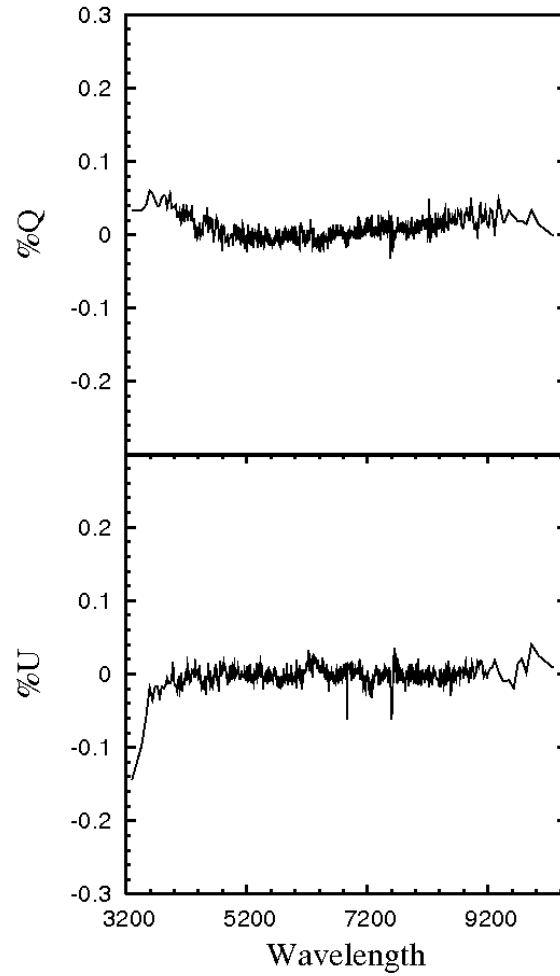


FIG. 10.— The residuals of our polarization low-state π Aqr data, binned to a constant (Poisson photon statistic) polarization error of 0.01%, are shown after subtracting the total ISP values listed in Table 5. The data exhibit a low level of residual polarization ($< 0.05\%$) in both the Stokes Q and U parameters and exhibits little structure outside of the regions in which the HPOL CCD sensitivity is low ($< \sim 4000$ Å and $> \sim 9500$ Å), providing confidence in the total interstellar polarization values we derived for π Aqr.

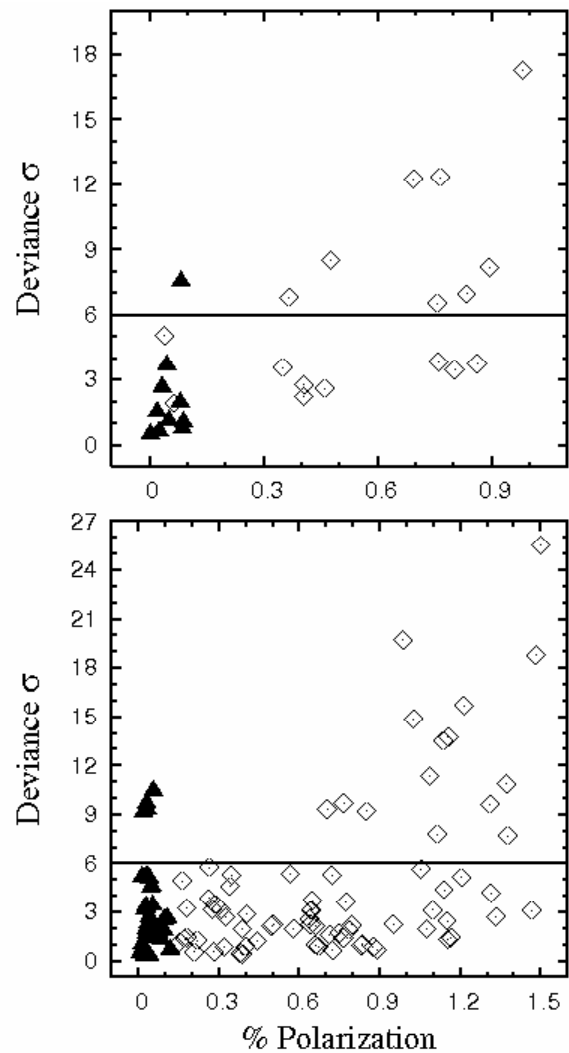


FIG. 11.— The absolute value of the error weighted deviation (deviance) of every V-band polarization observation of 60 Cyg (top panel) and π Aqr (bottom panel) from the best fit line in each star’s Q-U diagram (Figures 5 and 4) is plotted as a function of the magnitude of intrinsic polarization present in each observation. Filled triangles correspond to observations during the low (diskless) state of each star, while open diamonds correspond to observations during the high (disk present) state. For both 60 Cyg and π Aqr, the likelihood of observing a small-scale deviation in the polarization PA (from the bulk intrinsic PA of the disk) clearly increases with the magnitude of intrinsic polarization present. A simple false discovery rate analysis (see Section 4.2) confirms that this trend is statistically significant.

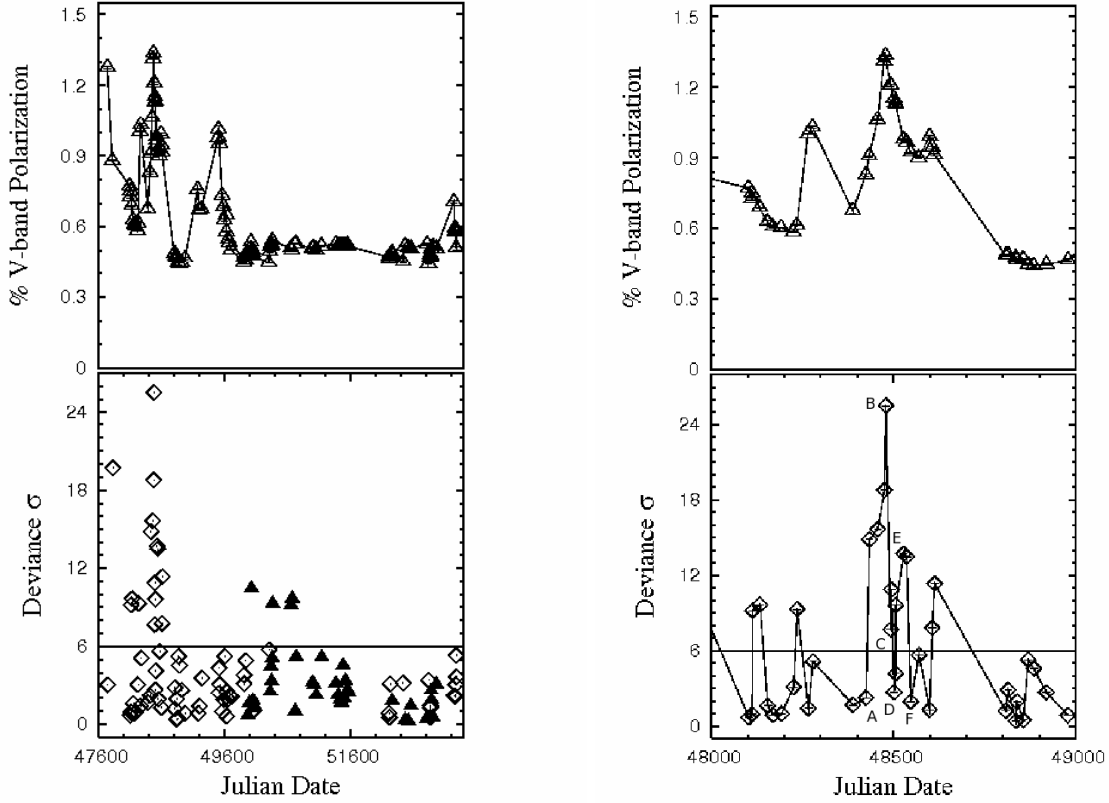


FIG. 12.— The absolute value of the error weighted deviation (deviance) of every V-band polarization observation of π Aqr from the best fit line in the star’s Q-U diagram (Figure 5) is plotted as a function of time (bottom panels) along with the V-band polarization as a function of time (top panel). The right-side set of figures, a zoomed view of the entire (left-side figures) dataset, illustrates that the majority of the large deviations in the deviance correspond to one of the major polarimetric outbursts observed in π Aqr. The rise of the first component of the outburst (points A to B, < 54 days) is similar to that of the second component of the outburst (points D to E, < 35 days), while the time-scale of the decline phase in each component is also similar (points B to C, < 13 days; points E to F, < 10 days). We interpret these data as evidence of departures from axisymmetry in the disk and postulate that they may be evident of newly injected disk material running into a density structure such as a spiral density wave (Figure 14), or of the injection and subsequent circularization of new blobs into the inner disk, similar to the phenomenon noted by Carciofi et al. (2007).

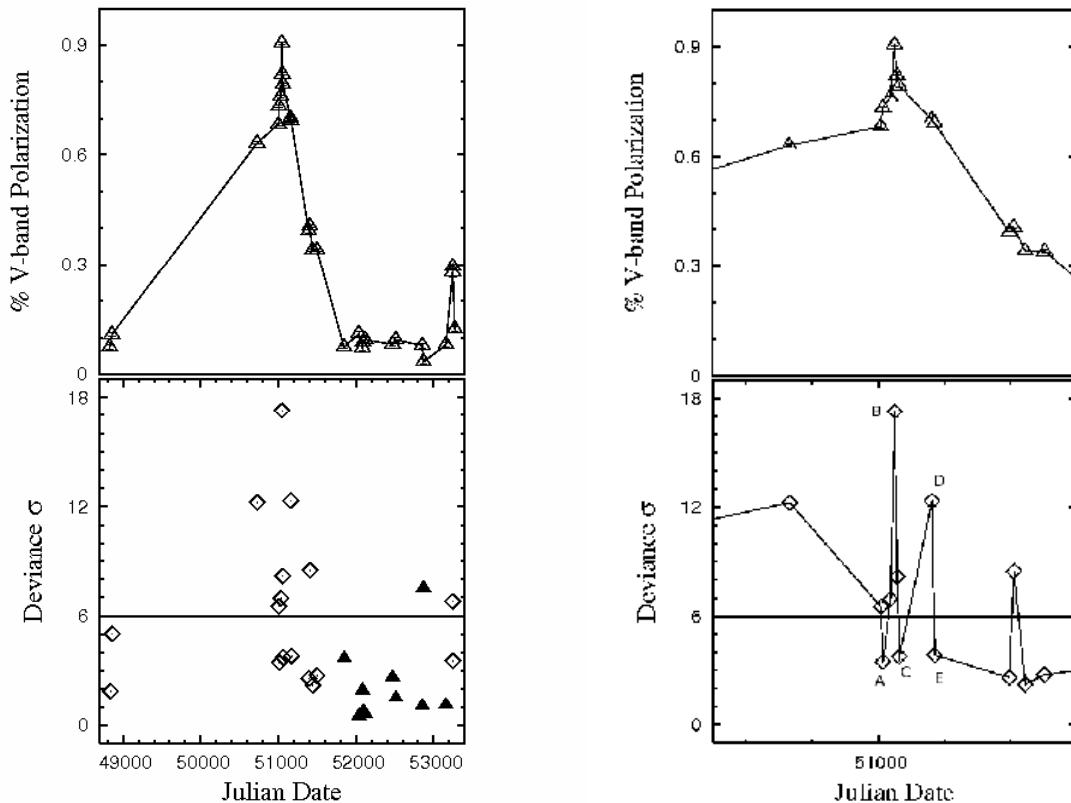


FIG. 13.— The absolute value of the error weighted deviation (deviance) of every V-band polarization observation of 60 Cyg from the best fit line in the star’s Q-U diagram (Figure 4) is plotted as a function of time (bottom panel) along with the V-band polarization as a function of time (top panel). The right-side set of figures, a zoomed view of the entire (left-side figures) dataset, illustrates that the majority of the large deviations in the deviance correspond to large polarimetric outburst observed in 60 Cyg. Both the time-scale of the rise in the outburst (points A to B, < 26 days) and the time-scale of the decline in the outburst (points B to C, < 14 days) are similar to the time-scales in the analogous phases observed for π Aqr. We interpret these data as evidence of departures from axisymmetry in the disk and postulate that they may evidence of newly injected disk material running into a density structure such as a spiral density wave (Figure 14) or of the injection and subsequent circularization of new blobs into the inner disk, similar to the phenomenon noted by Carciofi et al. (2007).

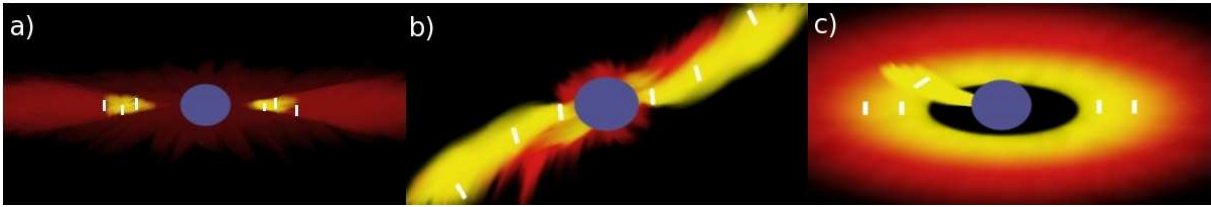


FIG. 14.— **a)** A simple cartoon image depicting an edge-on Be star disk, whereby the inner region of the disk responsible for producing the observed intrinsic polarization is shaded yellow and the bulk of the region responsible for producing the observed $H\alpha$ emission is shaded red. In the standard case of an axisymmetric disk, the maximum polarization vectors are oriented 90° from the plane of the geometrically thin disk. **b)** Departures from axisymmetry in the inner-region of the disk, such as those caused by the inject of one or more blobs which circularize into rings, would lead to intrinsic polarization vectors which are not all aligned perpendicularly with the bulk PA of the disk. We therefore speculate that one possible cause of the temporary (1-2 month) deviations in the intrinsic polarization PA values of both π Aqr and 60 Cyg is that blobs newly injected into the disk are created a warp-like structure in the inner disk. **c)** Alternatively, the observed deviations from axisymmetry could be caused by a blob (or series of blobs) launched from a non-equatorial latitude from the stellar photosphere, leading to the formation of a ring in an inclined (non-coplanar) orbit with respect to the semi-major axis of pre-existing disk material.